Unterschrift BetreuerIn

DIPLOMARBEIT

Influence of Noble-Metal Surfactants on Metal-Oxide Thin Film Growth

ausgeführt am Institut für Angewandte Physik
der Technischen Universität Wien

unter der Anleitung von
Univ.Prof. Dr.techn. Ulrike Diebold
Univ.Prof. Dr.techn. Mikk Lippmaa
und
Dr. Michele Riva

durch

Sarah Tobisch, BSc.
Matrikelnummer: 01614852

7th July 2023

Unterschrift StudentIn

Abstract

Metal-oxide thin films are widely used for a variety of emerging applications and technologies such as electronic-device building and photocatalysts thanks to their diverse physical and chemical properties. However, impurities, interstitials, and other defects can alter the electronic structure in semiconductor or insulator crystals used in photocatalysis, leading to in-gap states and thus limiting their potential usage in applications. Defect-related trapping of photoelectrons in oxide semiconductors remains a challenge in photoelectrochemistry, as the presence of trap sites and unoccupied in-gap states result in a loss of charge carriers due to recombination. This ultimately leads to a vastly shortened photocarrier lifetime, which in turn severely reduces the achievable energy efficiency of photocatalytic oxide materials. To avoid the problem of thermally generated defects, methods for growing thin films at low temperatures were developed. However, low temperatures greatly affect the kinetics of growth: due to a decreased mobility of surface atoms, the amount of time adatoms need to find thermodynamically stable lattice positions increases, leading to more bulk defects if not enough time was provided during deposition. Therefore, an atomically well-ordered and defect-free surface with a high mobility of surface atoms at low temperatures is essential for growing defect-free films.

In this thesis, the influence of Ir as a potential surfactant on $SrTiO_3$ homoepitaxial growth via pulsed laser deposition (PLD) was investigated using reflection high-energy electron diffraction (RHEED) to monitor the growth behavior and atomic-force microscopy (AFM) to examine the resulting surface morphology. In addition, the surface structure was analyzed using co-axial impact collision ion scattering spectroscopy (CAICISS). A difference in the growth mode when using Ir-doped $SrTiO_3$ was found for multiple deposition temperatures and a shorter periodicity of the RHEED oscillations when using Ir-doped $SrTiO_3$ compared to non-doped $SrTiO_3$ is reported. Step-flow growth is achieved earlier for Ir-doped $SrTiO_3$ at 800 °C. The segregation mechanisms of Ir during thin film growth of Ir-doped $SrTiO_3$ was investigated and a comparison with the literature was performed. The observation of clustering on the surface is only reported for a repetition rate of 1 Hz at 600 °C or for 0.5 Hz with multiple higher temperature depositions. In addition, the importance of well-defined substrate surfaces and the tight control of growth parameters such as the laser ablation repetition rate, the surface morphology and the Ir concentration in the deposited films was highlighted.

Kurzfassung

Dünne Metalloxidschichten werden dank ihrer vielfältigen physikalischen und chemischen Eigenschaften für eine Vielzahl neuer Anwendungen und Technologien, wie die Herstellung elektronischer Geräte und Photokatalysatoren, eingesetzt. Verunreinigungen, Zwischengitteratome und andere Defekte können jedoch die elektronische Struktur von Halbleiter- oder Isolatorkristallen, die in der Photokatalyse verwendet werden, verändern, was zu Bandlückenzuständen führt und somit ihre potentielle Nutzung einschränkt. Das defektbedingte Einfangen von Photoelektronen in Oxidhalbleitern ist nach wie vor eine Herausforderung in der Photoelektrochemie, da das Vorhandensein von Einfangstellen und unbesetzten Bandlückenzuständen zu einem Verlust von Ladungsträgern aufgrund von Rekombination führt. Dies resultiert in einer stark verkürzten Lebensdauer der Ladungsträger, was wiederum die erreichbare Energieeffizienz von photokatalytischen Oxidmaterialien stark reduziert. Um thermisch erzeugte Defekte zu vermeiden, wurden Methoden für das Wachstum dünner Schichten bei niedrigen Temperaturen entwickelt. Niedrige Temperaturen wirken sich jedoch stark auf die Wachstumskinetik aus: Aufgrund der geringeren Mobilität der Oberflächenatome, nimmt die Zeit, welche die Atome benötigen, um thermodynamisch stabile Gitterpositionen zu finden, zu, was zu mehr Gitterfehlern führt, falls während der Deposition nicht genügend Zeit zur Verfügung gestellt wurde. Daher ist eine atomar gut geordnete und defektfreie Oberfläche, mit einer hohen Mobilität der Oberflächenatome bei niedrigen Temperaturen, für das Wachstum defektfreier Schichten unerlässlich.

In dieser Arbeit wurde der Einfluss von Ir als potentielle oberflächenaktive Substanz (Surfactant) auf das homoepitaktische Wachstum von $SrTiO_3$ mittels Laserstrahlverdampfens (PLD) untersucht. Dabei wurde die Beugung hochenergetischer Elektronen bei Reflexion (RHEED) zur Überwachung des Wachstumsverhaltens und die Rasterkraftmikroskopie (AFM) zur Untersuchung der resultierenden Oberflächenmorphologie eingesetzt. Darüber hinaus wurde die Oberflächenstruktur mittels Ionenstreuspektroskopie (CAICISS) analysiert. Es wurde ein Unterschied im Wachstumsmodus für verschiedene Temperaturen bei der Verwendung von Ir-dotiertem $SrTiO_3$ und eine kürzere Periodizität der RHEED-Oszillationen bei der Verwendung von Ir-dotiertem $SrTiO_3$ im Vergleich zu nicht-dotiertem $SrTiO_3$ festgestellt. Step-Flow-Wachstum wurde für Ir-dotiertes $SrTiO_3$ bei 800 °C bereits früher erreicht. Die Entmischungsmechanismen von Ir während des Dünnschichtwachstums von Ir-dotiertem $SrTiO_3$ wurden untersucht und ein Vergleich mit der Literatur durchgeführt. Cluster auf der Oberfläche konnten nur für eine Pulsrate von 1 Hz bei 600 °C oder für 0,5 Hz nach mehreren De-

positionen bei höheren Temperaturen beobachtet werden. Darüber hinaus wurden die Bedeutung gut definierter Substratoberflächen und die akkurate Kontrolle von Wachstumsparametern, wie der Wiederholungsrate, der Laserablation, der Oberflächenmorphologie und der Ir-Konzentration in den abgeschiedenen Schichten, veranschaulicht.

Acknowledgements

First and foremost, I would like to thank Professor Mikk Lippaa (Sensei) for giving me the great opportunity to join his lab for half a year and learn a lot about metal oxide thin film growth and PLD. He was always encouraging and available for discussions about the research and his undying patience and curiosity were a great motivation.
Further I want to thank Michele Riva for his great support across the globe, always being available for questions or discussions and giving me very helpful advice during the writing process of this thesis.
I want to thank Ulrike Diebold for supervising me at TU Wien, therefore making my master thesis possible and giving me the opportunity to present my research in front of the entire Surface Physics Group.
I also want to thank everyone in Lippmaa lab - Taizo Mori, Tetsuhiro Hattori, Jiayue Ma, Yuchen Zhang, Jiwon Yang, Haotong Liang and Junko Nagayama - who made my time at the university unforgettable and allowed for many fun times next to many helpful discussions. Our small parties will not be forgotten. Special thanks go to Hattori-san, Yang-san and Ma-san for not only helping me settle in Japan, pay my rent and join university circles but also for the time spent together outside of the lab.
Huge thanks go to my dear friend Felix Tscharnutter who as a fellow physics student has always been a great support throughout my university years, in Japan and in Vienna - without you, I probably would not have gone to Japan!
A big thank you to the friends I made in Japan: Yuri Arakaki, Ken Takizawa, Chieko Yukita, Hikaru Suzuki, Kazuki Fujimura, Zen Somei and Yuuto Moronuki - you made my short time in Japan very special and unforgettable; from Tokyo to Kyoto to Hokkaido.
I want to thank Takuya Hiraga specifically, for the great times in Tokyo and during our short trip to Kyoto - you taught me a lot about the Kansai way of life.
Special thanks to my long-time university friends Florian Gisinger, Florian Weinzerl und Philipp Maier who greatly enriched my time as physics student.
Thank you, Ryunosuke Sannomiya, you were a great motivation during the later stages of my thesis writing and presentation.
I also want to thank all my friends who supported me during my thesis writing: Bao-Thy Thai, Sophia Unterberger, Alexander Firbas, Jasmina Cavkunovic, Elsa Bogg, Kristina Prvulovic, Sophie Kutschi, Leonard Cassidy and Sarah Bucci.
Last but not least, I want to thank my parents and my brother Adrian who supported me along my physics journey.

Contents

1 Introduction

1.1 Motivation

Metal oxides play an important role in developing new applications and technologies because of their diverse physical and chemical properties. A deep understanding of the surface structure and characteristics is crucial for many applications such as catalysis (photo-, electro-, and heterogeneous catalysis), as many relevant processes and reactions take place at surfaces. Thus, metal oxides have been intensively studied for decades by researchers from multiple backgrounds to understand and learn to control their variety of properties for multiple applications [1, 2].

Impurities, interstitials or other defects can alter the local electronic structure in metal oxides when introduced into the lattice, thus leading to defect states in the band gap that can be excited optically [3]. One example of defect engineering is the modification of the band gap of semiconducting oxide crystals in order to increase the absorption rate in the visible part of the solar spectrum for their use in photocatalysis [4]. However, defect-related trapping of photoelectrons in oxide semiconductors remains a challenge in photoelectrochemistry, as the presence of trap sites and unoccupied in-gap states result in a loss of charge carriers due to recombination. This ultimately leads to a vastly shortened photocarrier lifetime, which in turn severely reduces the achievable energy-conversion efficiency of photocatalytic oxide materials [5].

In complex oxides, crystal defects often have an extrinsic origin. For example, dopants may be intentionally added to a crystal or structural imperfections may be grown into a crystal due to stoichiometry errors or kinetic limitations. On the other hand, defects such as vacancies, interstitials or antisite substitutions may form even under thermodynamic equilibrium conditions [6]. Since such equilibrium defects have a certain formation energy, methods for growing thin films at lower temperatures have been explored to minimize the problems associated with thermally generated defects. However, low temperatures greatly affect the kinetics of growth: due to a decreased mobility of surface atoms, the amount of time adatoms need to find thermodynamically stable lattice positions increases, leading to more kinetically frozen lattice defects if the growth rate is too high [3, 7]. Therefore, an atomically well-ordered and defect-free surface with a high surface atom mobility at low temperatures is essential for growing defect-free films. Thus, a good knowledge of the kinetic and thermodynamic processes occurring on a crystal surface is crucial for controlling the surface morphology during thin film growth and the development of near-defect-free films. Since many electronic device or

catalysis applications require atomically smooth film surfaces, development of methods for optimizing film growth remains an active field of research. One choice for improving the structural quality of thin films is to use a suitable surfactant, a substance which can alter the growth conditions. A surfactant can decreases the strain energy and increases spreading behavior, thus promoting the growth of flat surfaces [8]. Another mechanism is the suppression of intra-layer mass transport or promotion of inter-layer mass transport, resulting in a lower roughness of the surface [9].
A well-suited approach to study the properties of metal oxides, is to reduce the complexity of a real system by studying well-defined single-crystal surfaces under highly controlled conditions. In addition, many surface-analysis techniques require ultra-high vacuum conditions to function properly.
Studies have shown that the properties of a crystal surface can differ significantly from bulk properties. The surface energy of a crystal can often be minimized by shifting surface atoms away from their bulk positions, forming a reconstructed surface, which is characterized by specific symmetries, coordination, and arrangement of the surface atoms. This also holds true for many metal oxides where the concentration of defects such as oxygen vacancies or cation interstitials depends on the method of preparing the surface [10, 11].

Pulsed laser deposition (PLD) stands out as one of the best methods for growing high-quality oxide thin films and is used in various fields of research as it enables control over the crystal structure, orientation and stoichiometry among other crystal parameters. In combination with reflection high-energy electron diffraction (RHEED), PLD is capable of producing thin films with atomic-layer accuracy. With a suitable deposition source, it is possible to grow complex, multi-element materials. However, the properties of thin films grown by PLD depend on a multitude of control parameters which makes the optimization process for obtaining smooth high-crystallinity thin films tedious: it involves many modifications until the desired result is achieved. Atomic-force microscopy (AFM) studies have demonstrated the importance of tuning the PLD parameters to control the surface morphology of the grown films [12]. Not only the PLD parameters can be varied to achieve different films, but the composition of the target material may also influence the structure by introducing different levels of doping.
The incentive for this project was to explore the influence of noble-metal doping on the growth dynamics of perovskite-type oxides. Strontium titanate ($SrTiO_3$) was used as a model system. Noble-metal species were co-deposited during homoepitaxial growth

by using an Ir-doped $SrTiO_3$ target to study the effect of the noble-metal atoms at the film growth front on the thin film growth dynamics and surface morphology compared to non-doped homoepitaxial growth. Previous research suggests that noble-metals co-deposited with an oxide can act as a surfactant, increasing the migration length of surface atoms and therefore improving surface flatness [5]. When growing Ir nanopillars embedded in $SrTiO_3$, oxide adatoms have been found to conglomerate around the nanopillars and form pyramid-like structures, suggesting that the co-deposition of noble metals with an oxide greatly changes the migration length of oxide species leading to an overall flatter oxide surface. However, this effect has not been well studied in the context of oxide film growth [13].

Therefore, the objective of this thesis was to investigate this phenomenon by growing homoepitaxial films of $SrTiO_3$ using PLD and monitoring the growth using RHEED as well as studying the surface morphology via AFM after deposition and comparing the results of using pure-$SrTiO_3$ ablation targets to using noble-metal-doped targets. In addition, the thermodynamic and kinetic processes occurring on the surface upon deposition are studied in regard to different growth conditions, to gain insight into the mechanisms involved in $SrTiO_3$ thin film growth.

1.2 Surface morphology and growth kinetics

For decades, the description of the mechanisms involved in epitaxial growth has been a topic of active research and remains a challenging problem to this day [14, 15]. Especially the questions of how the film surface behaves upon deposition and which models can accurately describe these processes are still heavily debated [16, 17].

In general, the crystal growth can be described in terms of a combination of thermodynamic and kinetic aspects. The thermodynamic approach to crystal growth is used to describe systems that are either in or close to thermodynamic equilibrium. This means that the instantaneous deposition rate is much smaller than the surface diffusion. However, growth itself needs to be a non-equilibrium process since the opposing atomic processes at thermodynamic equilibrium would proceed at equal rates, thus no net growth would be possible [18]. Due to local fluctuations from the equilibrium, nucleation occurs which leads to a phase transition from the gas or liquid to the solid phase [16].

The most common growth modes of thin film epitaxy are shown in Figure 1. The occurrence of these growth modes can be, in terms of thermodynamics, qualitatively attributed to the surface free energies of the film surface γ_f, the substrate surface γ_s

and the interface between them γ_I. The island growth mode is characterized by small clusters directly nucleating onto the substrate surface upon migration. Due to stronger bonding between the film atoms compared to bonding to the substrate and an increased interface surface energy γ_I, 3-dimensional island growth is preferential. However, if the surface energy of the saturated substrate surface is lower than that of the pristine one, the adatoms are bound more strongly to the substrate surface and the growth will proceed in layer-by-layer fashion. The growth of the second atomic layer will only be initiated after the previous layer has been completed, leading to 2-dimensional growth. The Stranski-Krastanov mode is an intermediate case. The growth initially proceeds layer-by-layer until the built-up stress due to lattice mismatch during heteroepitaxial growth leads to an elastic energy which increases with film thickness. After the critical layer thickness has been reached, the growth proceeds in island growth on top of the film [19].

It should be emphasized that these models assume monoatomic thin film growth where average surface and interface energies can be defined. In the case of oxide film growth where multiple types of atoms are present, other aspects such as terminating layers and cation segregation need to be considered, thus defining surface and interface energies becomes more difficult.

Kinetically driven growth modes due to diffusing atoms also need to be considered. Large interlayer mass transport leads to layer-by-layer growth whereas small interlayer mass transport results in multilayer three-dimensional growth.

Step-flow growth is a type of two-dimensional kinetic growth and can only occur when pre-existing steps are available on the surface. If the surface diffusion length of the adatoms is much larger than the average terrace width of the substrate surface, the growth may proceed in step-flow growth. Growth occurs at the step-edges of terraces and leads to fewer surface defects than nucleation via layer-by-layer growth [19].

In heteroepitaxial growth, the elastic strain in the film due to the lattice mismatch can influence the surface morphology evolution. The stress increases with the film thickness until the critical film thickness is reached and lattice dislocations are introduced to relieve the mismatch strain as this change in the elastic energy is comparable to the increase in interface energy, thus changing the growth mode [16]. One possible mechanism to relief this strain is the Stranski-Krastanov mode.

In addition, for oxides, oxidation kinetics plays a crucial role which depend on a variety of conditions such as the substrate temperature, the oxygen background pressure and the growth rate [20].

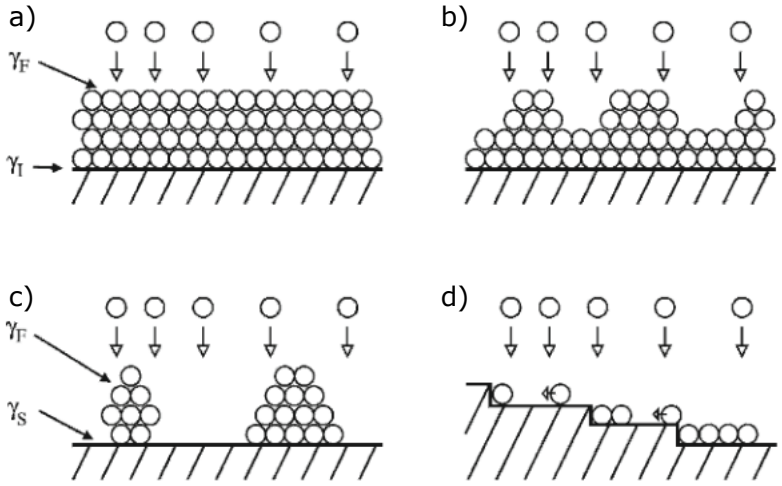

Figure 1: Schematic diagram of various growth modes: a) layer-by-layer, b) Stranski-Krastanov, c) island growth and d) step-flow growth. Adapted from [16].

In PLD, a laser beam is focused onto a target, leading to a high energy density in a small volume. If the energy is high enough, a plasma of highly energetic target particles is formed which will expand rapidly, forming a plasma plume which is directed onto the surface of the substrate. A more detailed description of the PLD process can be found in Section 2.2.

The process of film growth by PLD is not taking place close to thermodynamic equilibrium, thus the previously introduced thermodynamic description is not sufficient to describe the growth mode. A combination of kinetic effects and thermodynamics have to be considered.

Due to limited surface diffusion, the deposited material cannot rearrange in such a way to fully minimize the surface energy. In addition, the adatom density is very high just as the plume reaches the surface. Nucleation of the particles occurs when the concentration of the solute, in this case the adatoms from ablated target material, is sufficiently higher than the equilibrium solubility of the solid. This state is then called supersaturation. This high supersaturation of the vapor during a deposition pulse leads to a high nucleation rate [21].

Several models have been proposed to describe nucleation and thin film growth processes. Typical processes that these models need to include are: a) the flux of atoms onto a substrate surface which is described by the deposition rate, b) diffusion of adatoms on the surface, c) formation adatom dimers, d) attachment of adatoms to existing islands, e) detachment of adatoms from existing islands, f) diffusion of adatoms along

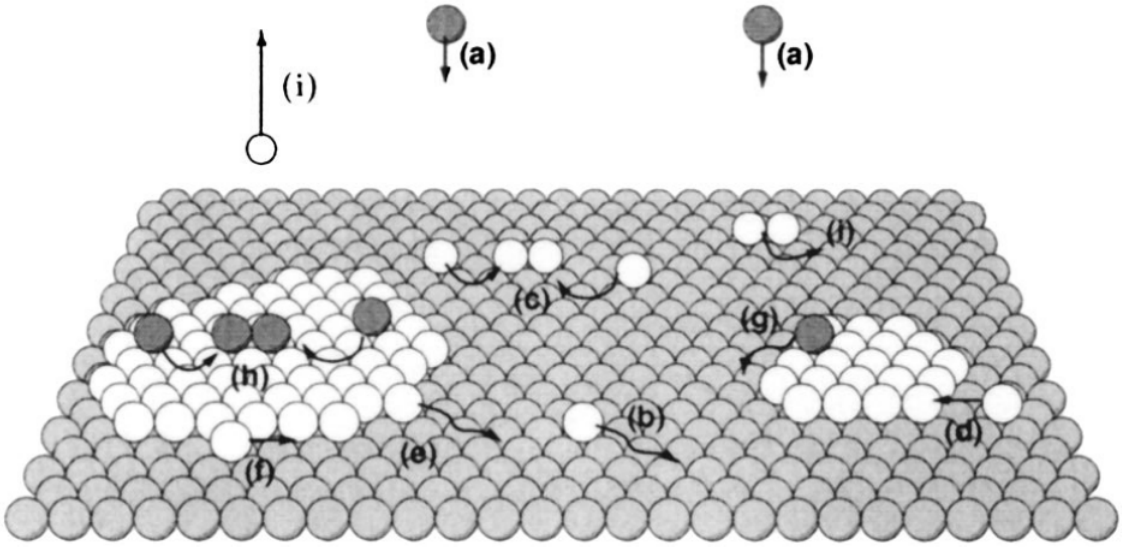

Figure 2: Atomistic processes that can occur during thin film growth such as a) incoming adatoms getting deposited on the substrate surface, b) adatoms diffusing on the surface, c) dimer formation, d) adatoms attaching to and e) detaching from existing islands, f) adatoms diffusing along island edges, h) adatoms getting deposited on top of existing islands, g) adatoms descending an island edge, h) adatoms nucleating on top of existing islands and i) adatoms re-evaporating. Another process which is not included in the figure is the diffusion of deposited atoms into the substrate. Reprinted from [22].

island edges, h) deposition of adatoms as well as diffusion on top of existing islands and g) descent of adatoms from islands [22]. For high temperatures, the evaporation of adatoms is also possible. These atomistic processes are sketched in Figure 2. One possibility to model these processes is the usage of rate equations which describe the time evolution of mean-field quantities such as the adatom density and the island size. The selection of so-called capture numbers which are used in the rate equations to describe dimerization or capture of an adatom by an island, have been subject of intensive study. The advantage of rate equation is that they are easy to formulate and can be numerically solved. However, a major drawback is often a lack of spatial information and therefore not leading to information on surface morphology. Some attempts have been made to find capture numbers which do encode spatial information [22, 23]. In addition, some models using rate equations have been specifically designed to describe thin film growth by PLD [24].

Another method is the level-set method (island dynamics) which describes the formation and evolution of island boundaries. The model can resolve individual atomic layers but is continuous in lateral directions and can therefore treat growth on arbitrarily large

lateral length scales. The advantage of this method is that it can describe fast atomistic processes without drastically changing the numerical time step in the simulation which would increase the computational cost [25].

Alternative approaches make use of kinetic Monte Carlo simulations (KMC) which in each step generate a random sequence of microscopic processes with respect to their individual probabilities. The main difficulty is to decide which parameters should be included in the simulation. The time step for the simulation is crucial, as it should be determined to accurately capture the fastest processes. This is especially critical for PLD due to fast diffusion times and highly energetic particles. Therefore, without using simplified models, one can only model the growth of a few monolayers. Modifications of kinetic Monte Carlo simulations have been proposed to overcome these limitations. Gabriel *et al.* [26] have presented a model for layer-by-layer growth by PLD which assumes that, in the fast-diffusion limit, the deposited material can be described as a 2D gas of non-condensed material instead of accounting for a full random walk. This method successfully speeds up the computation and has been recently applied [24] to describe interlayer transport in $SrTiO_3$ homoepitaxy. Both interlayer transport (diffusion of atoms across a step-edge) and intralayer transport (diffusion of atoms on a flat terrace) can greatly influence the growth mode [19].

In homoepitaxial growth, strain induced by lattice parameter misfit and different thermal expansion coefficients can be neglected since the crystalline structure of the deposited material is identical to that of the substrate. The growth is determined by the surface diffusion coefficient D_S of the adatoms, the sticking probability of an adatom reaching the edge of a terrace and the energy barrier E_S for adatoms to reach the lower edge of a terrace. The surface diffusion coefficient determines the average distance an atom can migrate on a flat surface before being trapped on a site. This distance is called the diffusion length l_D and is generally defined as

$$l_\mathrm{D} = \sqrt{D_\mathrm{S}\tau}, \tag{1}$$

where τ is the time the adatom resides on the surface before re-evaporation. The surface diffusion coefficient D_S is defined as

$$D_\mathrm{S} = \nu a^2 \exp\left(-\frac{E_\mathrm{Diff}}{k_\mathrm{B}T}\right), \tag{2}$$

where ν is the attempt frequency of the adatom for jumping to the next neighboring site, a the characteristic jump distance and E_Diff the activation energy for diffusion [16].

The exponential dependence in Eq. (1) highlights the importance of the deposition temperature for diffusion, as high temperatures facilitate migration on the surface of the substrate. Flat, smooth film surfaces can only be achieved if there exists a sufficient surface mobility. Island morphologies are also highly dependent on island-edge diffusion, as high mobility leads to the formation of more compact island shapes whereas low mobility leads to rough, fractal-like islands. The diffusion-limited-aggregation model (DLA) describes the limiting case of (almost) zero island-edge mobility where every diffusing adatom sticks to the first island upon impact [27]. In that case, growth of fractal islands can occur which has been shown by scanning tunnelling microscopy (STM) [28].

The potential energy curve for an adatom at a step-edge can be considered as taking on an asymmetrical form, as seen in Figure 3. The adatom reaching the edge from the lower terrace would have a higher probability of sticking to the step-edge because of its higher coordination and binding energy. Therefore, an adatom trying to ascend a step would require additional energy. Hence, this type of diffusion is often neglected. Crossing a step from the upper side will temporarily decrease the coordination of an adatom and is thus energetically less favourable. This additional barrier is known as the Ehrlich–Schwoebel barrier E_{ES} and has to be overcome by an adatom when moving down a terrace.

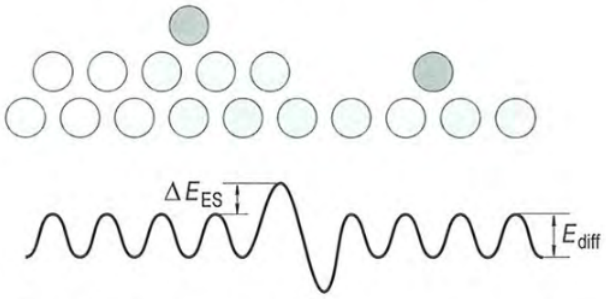

Figure 3: Schematic illustration of the asymmetric potential energy around an atomic step. ΔE_{ES} denotes the Ehrlich-Schwoebel barrier, which has to be overcome by an adatom in addition to the diffusion barrier E_{diff} when moving down a step-edge. Reprinted from [19].

For step-flow growth the diffusion length l_{D} is larger than the average terrace width. Therefore, interlayer mass transport is not essential for step-flow growth since adatoms reach a step before the nuclei on a terrace reach the critical size. In other words, due to a high surface diffusion, the nuclei dissolve before the stabilizing radius is reached. In contrast, for migration lengths below the average terrace width, the Ehrlich-Schwoebel

barrier determines whether layer-by-layer growth or three-dimensional growth takes place [19]. A high interlayer mass transport is required for the adatoms to be able to migrate across an island edge and reach a lower terrace, thus forming a single layer [29]. When using PLD, the high deposition rate of the species is followed by a much longer period without deposition. The amount of deposited species and their interaction with the surface of the substrate determines the mode of nucleation of the particles. Since the adatom saturation is high during a deposition pulse, the critical island size is expected to be small, thus these nuclei become unstable during the recovery period and dissociate into migrating atoms which can attach to step edges or other islands [30]. Thus, the activation energy corresponds to the energy needed to remove an atom from the edge of an island. For that reason, the value for the activation energy E_A is not only related to the diffusion of particles but also to the diffusion of the clusters [14].

1.3 $SrTiO_3$ (STO)

Strontium titanate ($SrTiO_3$) has a cubic crystallographic structure with a lattice constant $a = 3.905$ Å at room temperature and a thermal expansion coefficient of $\alpha = 9 \times 10^{-6}$ K^{-1}. The unit cell is shown in Figure 4a.

$SrTiO_3$ is a popular choice as a substrate material for the growth of perovskite oxide films because of its small lattice mismatch with many other perovskites and due to its dielectric properties, such as paraelectricity and a high relative dielectric constant [31]. In recent years many interesting phenomena using the $SrTiO_3$ system have been discovered, such as it being an oxide superconducting material with the lowest carrier density, the migration of oxygen vacancies at $BaTiO_{3-\delta}/SrTiO_3$ interfaces or the occurrence of a ferromagnetic metallic phase and an antiferromagnetic insulating phase in strained $SrRuO_3/SrTiO_3$ superlattices [32].

Point defects such as impurities, oxygen vacancies or interstitials are present in all real oxide systems. Most commercial $SrTiO_3$ single crystals are reported to have a purity $> 99.98\%$ (Shinkosha, Yokohama, Japan). However, the impurity concentration is in general not precisely known and can vary between different crystals from the same manufacturer. These impurities can affect properties such as charge carrier transport and photoconductivity in a significant manner [33].

$SrTiO_3$ is a promising candidate material as a photoelectrode for photoelectrochemical water splitting as it is stable in water and commercially available as high-quality $SrTiO_3$ single crystals with moderate price. However, due to its large band gap (3.25 eV), only light in the ultraviolet (UV) regime of the solar spectrum can be absorbed, which is only a small fraction of the sunlight, thus leading to low energy-conversion efficiency [34]. Extensive research on band-gap engineering has been conducted to extend the absorption range into the visible-light spectrum by introducing suitable impurities. Doping $SrTiO_3$ with metals or non-metals such as Ir or Rh leads to a reduction of the bandgap and a photocatalytic response upon irradiation with visible light [35]. However, this can in turn suppress the photocatalytic activity due to partially occupied impurity states that can act as recombination centers for electron-hole pairs [36]. Since the photogenerated carriers in the bulk need to reach the surface to react with water, the carrier lifetime has to be long enough to make migration to the surface possible. The photocarrier lifetime of $SrTiO_3$ is of the order of 100 ps or less, depending on the type of doping [37]. Thus carriers cannot reach the surface in time to react.

Any impurity in a crystal that forms electronic states within the band gap or close to the valence or conduction band edges can affect the transport behavior of charge carri-

ers and thus the photocatalytic activity of the material. From a band-gap engineering point of view of hydrogen-evolution photocatalysts, it is useful to introduce impurities that create new in-gap states that lift the valence-band maximum without lowering the conduction-band minimum, thereby bringing the energy gap closer to the water redox potential separation of 1.23 eV while allowing electron transport from the conduction band of the semiconductor to water [33]. Oxygen vacancies are another type of defect that can strongly influence the electronic properties of a material. Since oxygen in $SrTiO_3$ exists mainly as an O^{2-} ion, the presence of oxygen vacancies leads to n-type doping. It is assumed that the main reason for the short carrier lifetime is related to trapping at shallow trap sites due to oxygen vacancies or other defects with electronic in-gap states close to the bottom of the conduction band [5].

Even in non-doped $SrTiO_3$ the dominant cause for carrier loss is trap-related carrier recombination, since the photoconductivity shows a sharp increase at low temperatures at around 35 K [7]. The so-called sensitization model for semiconductors assumes two types of in-gap states: (i) sensitizing centers close to the upper edge of the valence band and (ii) fast recombination centers in the mid-gap region. At low temperatures, when exposing the semiconductor to UV light, the holes are captured by sensitizing centers and have a longer lifetime than holes trapped by the fast recombination centers. This leads to a lower recombination of the carriers. Therefore, at higher temperatures the holes which are trapped at sensitizing centers are thermally released and can migrate to the fast recombination centers, thus resulting in a loss of photoconductivity [7].

The hole trap centers are presumed to be caused by Sr vacancies, which are always present, even in pristine $SrTiO_3$ due to the low formation energy of a V_{Sr} defect. Growing thin films at low temperatures might reduce the number of such defects and thus the probability of carrier recombination at defect sites, but lower-temperature growth comes at the cost of reduced mobility of the deposited adatoms, which may also create defects in the crystals at practical growth rates. As seen in Section 1.2, the growth kinetics depends exponentially on the temperature. This means that, at low temperatures, adatoms require more time to find step-edges and form flat surfaces. Since the temperature dependence of the migration rate is exponential, it is easy to understand that reducing the growth temperature leads to a major reduction in the adatom diffusivity. Thus, trying to keep the ratio of deposition to diffusion constant can result in impractically slow growth rates. In practice, limited migration time leads to a higher density of defects, such as antisite substitution, stacking faults, etc., which again lead to a higher photocarrier recombination rate and strongly reduced photocatalytic activ-

ity. Mechanisms for growing thin films at lower temperatures are thus crucial for the development of defect-free $SrTiO_3$ model systems for photocatalysis.

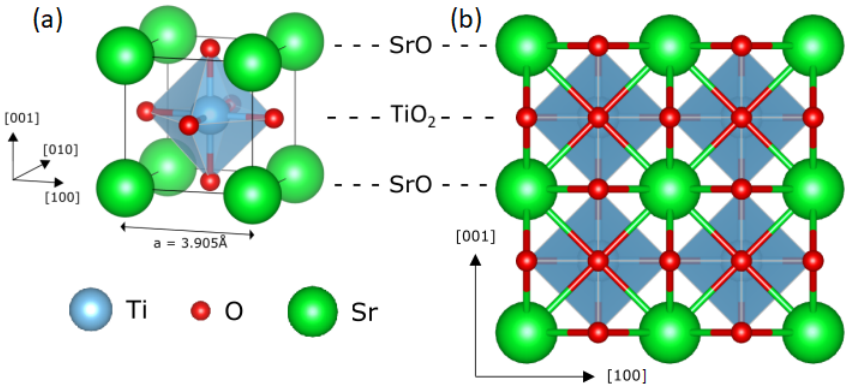

Figure 4: a) The cubic $SrTiO_3$ unit cell. b) Side view of the $SrTiO_3$-(001) bulk-truncated surface.

The $SrTiO_3$-(001) structure consists of alternating layers of charge-neutral SrO and TiO_2 layers (see Figure 4). Methods for preparing atomically flat $SrTiO_3$-(001) surfaces have been studied for decades. One of the first successful methods for preparing an atomically smooth TiO_2-terminated surface was proposed by Kawasaki *et al.* [38] by treating the surface with an NH_4F-buffered HF solution (BHF) with different pH values. The solution selectively etches the SrO layers, and therefore leaves purely TiO_2-terminated surfaces. Due to uncontrolled etch defects appearing if the correct polishing and annealing conditions were not met, a more refined technique was developed by Koster *et al.* [39]. This technique uses the formation of an intermediate strontium hydroxide complex before BHF etching to obtain TiO_2 terminated surfaces. However, it should be noted that using HF-etching results in F being unintentionally doped into O sites leading to contamination of the surface [40]. By using friction force microscopy, it was possible to determine the terminating layer of a terrace on the $SrTiO_3$-(001) surface locally using the friction contrast. In addition, the termination was identified by looking at the step edge contours in scanning force microscopy [41]. This knowledge is especially crucial at interfaces, since properties such as the charge-carrier density significantly changes depending on the termination. For example, $LaAlO_3$ films grown on TiO_2-terminated crystals form metallic interfaces whereas SrO-terminated interfaces are insulating [42]. In the diffusion model discussed in Section 1.2, the diffusion barrier very likely also depends on the termination. A difference in the migration barrier of an oxygen vacancy between SrO and $SrTiO_3$ has been shown in Figure 4 of Ref. [14]. The

selection of the surface termination is therefore an important step before film growth. The $SrTiO_3$-(001) surface also shows a variety of surface reconstructions, which can severely alter the properties of the surface, making it insulating, polar or with mixed terminations. Previous research concludes that polished and annealed samples generally show a (1×1) surface periodicity [43]. Annealing under oxidizing conditions can lead to the creation of Sr vacancies which can in turn lead to the formation of SrO-rich phases at the surface [6]. Highly reducing conditions also lead to large concentrations of oxygen vacancies, thus the annealing process must occur in oxygen to prevent the formation of oxygen deficiencies [6, 44]. $SrTiO_3$ surface preparation is often carried out using an oxygen pressure of 10^{-6} Torr which does generate oxygen vacancies, however, the oxygen can be restored by annealing the film in air at around 400 °C for multiple hours.

However, most reports rely on electron-diffraction techniques such as LEED to determine the surface phase, which are also influenced by subsurface layers. Recent work suggests that a bulk-terminated surface cannot be generally assumed as atomically resolved nc-AFM shows the appearance of both SrO- and TiO_2-terminated domains and charge defects as well as disordered top layers at higher temperatures [45].

The $SrTiO_3$-(001) surface remains a complex system with many aspects which are not well-understood and it will require further research to tackle the existing questions and challenges.

2 Experimental methods

2.1 Reflection high-energy electron diffraction (RHEED)

Reflection high-energy electron diffraction (RHEED) is an important analysis tool for obtaining information about the periodic arrangement of surface atoms because of its high surface sensitivity. Due to the grazing incidence measurement geometry and compatibility with a wide range of background gas pressures, this technique has become an indispensable tool for monitoring the process of thin film growth.

2.1.1 Basic principles

In RHEED, an electron beam with energies on the order of 10–50 keV is directed at a sample surface under grazing incidence of a few degrees. This shallow angle results in the electron beam only interacting with the first few atomic layers, making this technique very surface sensitive. The diffracted beam is then directed at a phosphor screen where the characteristic RHEED pattern for the sample can be observed.
The construction of RHEED patterns is usually explained as an elastic scattering event in reciprocal space. The magnitude of the wave vector of the incident beam is given by

$$k_0 = \frac{1}{\hbar}\sqrt{2m_0E + \frac{E^2}{c^2}}. \tag{3}$$

The relativistic correction can often be neglected for qualitative analysis since it only contributes about 3%. The penetration depth of RHEED is of the order of a few atomic layers, which means that the periodicity of the bulk can usually be neglected. That way, the reciprocal lattice can be approximated by one-dimensional continuous rods along the z-axis, perpendicular to the surface. The reflection which results from the intersection of the rods with the Ewald sphere occurs along the Laue circles, centered parallel to the position of the direct beam spot which results from the part of the electron beam that misses the substrate surface. The (00) spot, which is often also called the specular reflection spot in the literature, is situated at the intersection of the zeroth-order Laue circle with the (00) rod. A schematic view can be seen in Figure 5 [46]. The diffraction pattern observed in RHEED can give important insights into the morphology and stoichiometry of the sample surface. If the surface has a finite number of domains whose sizes are smaller than the coherence length of the electrons beam, the RHEED pattern will exhibit various features deviating from the ideal surface pattern such as broadening of the reciprocal rods [47]. This leads to the intersection of the

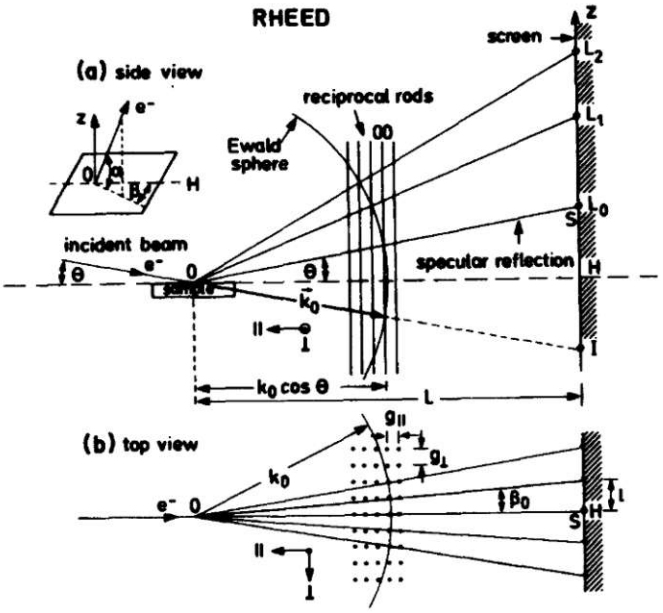

Figure 5: Ewald sphere construction and RHEED diffraction geometry. Reprinted from [46].

Ewald sphere with the reciprocal rods becoming ellipses, thus resulting in a broadening of the diffraction spots often referred to as streaks. Schematics of the different types of features displayed in RHEED can be seen in Figure 6. Two-level stepped, multileveled stepped or vicinal surfaces show more complex shapes of the reciprocal rods, since the electron waves reflected from the steps interfere with each other (Figure 6c-e).
Conducting RHEED on an ideal crystalline surface would lead to sharp diffraction spots located on the Laue circles. In any real setup, there will always be deviations from the ideal position due to defects or rough surfaces, resulting in the aforementioned streaks. Dynamic scattering effects such as the appearance of Kikuchi lines, which are created from diffuse-scattered electrons, should also not be neglected. While measuring the intensity of diffraction spots, intersecting with Kikuchi lines should be avoided because of the additional contribution to the diffracted intensity caused by the Kikuchi lines.
Optimizing the incident angle and setting up the RHEED hardware, such as the filament, magnetic coils or pinhole for focusing, in accordance with the used chamber pressure is crucial for obtaining sharp and symmetric diffraction patterns. A view of the PLD chamber with the RHEED setup used for this thesis can be seen in Figure 8. The setup itself is described in more detail in Section 2.2.2.

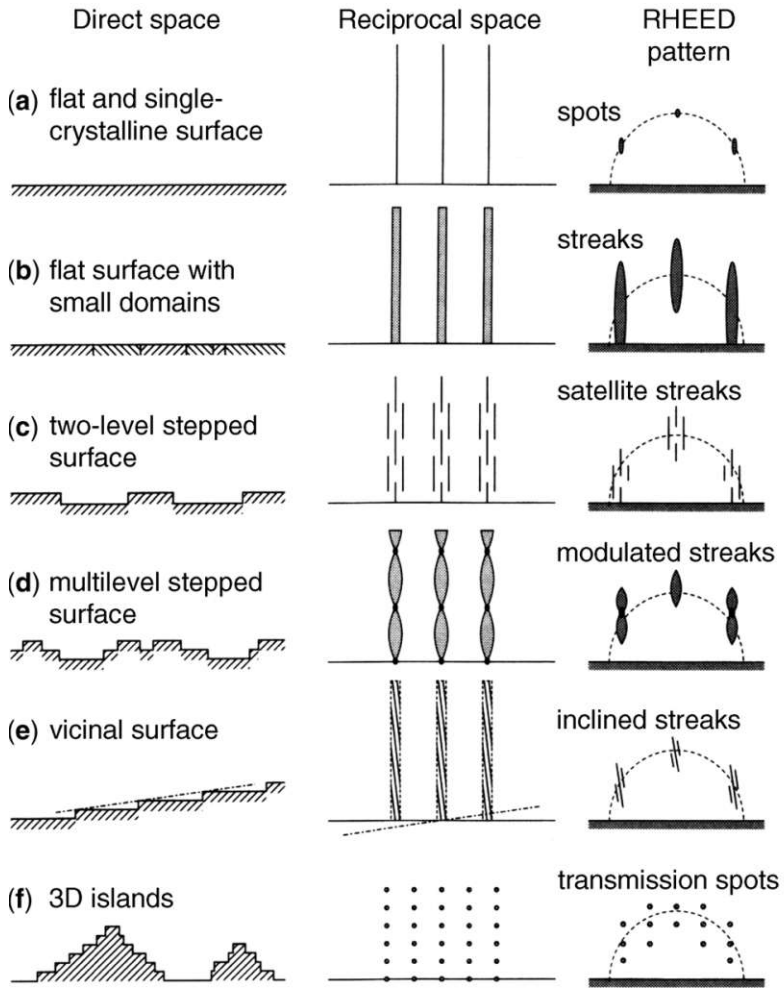

Figure 6: Schematics of different types of features seen in RHEED patterns due to various surface morphologies. Adapted from [47].

2.1.2 RHEED intensity oscillations

RHEED is primarily used to acquire qualitative information about the crystallinity of the substrate surface and changes concerning growth modes or surface reconstructions during thin-film growth. Monitoring the temporal variations of the diffraction spots during deposition can yield valuable information about the film-growth dynamics.
If the glancing angle equals the exit angle of an electron, this diffraction spot is called specular spot. To monitor the growth of atomic layers on a surface, time-dependent changes in the intensity are measured and recorded. If there is an atomic step on the surface, there will be reflections from the upper and the lower terrace, resulting in a phase difference between them. By measuring the intensity of the specular spot under off-Bragg condition (out-of-phase), the two electron waves will interfere destructively

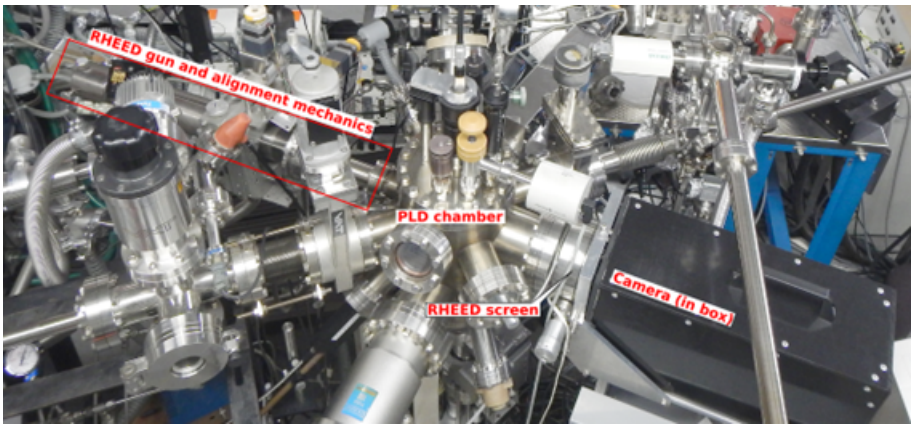

Figure 7: View of the PLD chamber with the RHEED electron gun, RHEED screen and camera.

and lower the intensity of the specular beam. This can be used to distinguish atomically flat surfaces from stepped or rough surfaces [47].

The intensity of the specular reflection is sensitive to the surface roughness of a crystal. During thin film growth, an oscillatory behavior is often seen, which can be attributed to the growth modes discussed in Section 1.2. In island growth the RHEED intensity will drop immediately upon deposition, due to scattering and reflections from islands and terraces. As this growth mode leads to three-dimensional island growth, the intensity will never recover. A periodic intensity variation of the diffraction features during deposition with the period corresponding exactly to the growth of one layer on a surface is generally thought to be a feature of two-dimensional layer-by-layer growth [17, 48, 49]. However, the question of when one layer has truly been completed has been the topic of many publications and many models have been used to gain a deeper understanding of the mechanisms involved in the growth modes. It has been shown that dynamical diffraction theories which include multiple scattering processes (e.g., the layer interference model) agree well with experimental results [46]. However, even simpler models like the kinematic scattering approximation or the phenomenological step-density model have been used to describe RHEED intensity oscillations quite well [50]. Both models rely on a single parameter such as the coverage or the step density to describe the evolution of the surface morphology.

In the step-density model, the specular intensity depends only on the number of steps on the surface. Since every step acts as a diffuse scattering center, the specular intensity is low when the step density is high. As more adatoms are deposited on the surface and the layer gets completed, the number of steps on the surface is again reduced, leading

to a recovery of the specular intensity. In the ideal case, the full surface is recovered, thus the intensity returns to its original value. Therefore, in this model the specular RHEED intensity is a measure of the density of steps at the surface. During deposition, an oscillation of the step density occurs due to migration of the deposited species, leading to nucleation and coalescence of islands [16]. The migration length is determined by the average island size which depends on the coverage and the nucleation density [29]. When using molecular-beam epitaxy, the morphology of the surface changes due to nucleation and coalescence, leading to periodic changes in the RHEED intensity when completing a layer. This behavior is also present for PLD, however, due to the interrupted growth, the damping and recovery of the oscillations which happen on a smaller time scale become visible. During PLD, the time between two deposition pulses enables adatoms to migrate on the surface and potentially diffuse to step edges of existing islands. According to Stoyanov *et al.* [51], the RHEED intensity relaxations can be attributed to particles diffusing on the surface layer and getting incorporated at step edges of islands and terraces. The step density evolution is therefore directly correlated to the diffusivity and average travel distance of the particles. However, its inconsistency with diffraction theory and lack of arguments from scattering theory has been criticized multiple times [48]. One major point of criticism is that both the coverage and the step density affect the RHEED intensity. Calculations have shown that in high density regimes, the increase of the step density at constant coverages correlates with an increase of the specular beam intensity, contrary to the step density model [52].
Nonetheless, the step-density model remains a popular choice for explaining the evolution of RHEED oscillations. Blank *et al.* [15] have used the step density model to describe the intensity variation during layer-by-layer homoepitaxial growth of $SrTiO_3$ and to obtain the relaxation time by fitting the intensity for each laser pulse for different temperatures, coverages and pressures by approximating the intensity via the following function

$$I \approx I_0(1 - e^{-t/\tau}). \tag{4}$$

By plotting the relaxation times as a function of the temperature for different coverages, which was found to be of linear nature, they were able to calculate the activation energy from Eq. (4). When using PLD, this means that for the comparison of the relaxation times it is crucial to measure the pulses occurring at the same coverage.
Both the step density model and the kinematic approximation predict that the RHEED intensity oscillations are out of phase with the surface roughness, which has been shown in experiments [17] [49]. However, research has also shown that this is not always the

case since the intensity can decrease at the start of deposition and recover to an intensity higher than at the beginning [14]. Sullivan *et al.* [17] have indicated that it is not possible to determine from the RHEED oscillation phase alone when a layer has been completed. Unlike in x-ray reflectivity, the oscillation phase for RHEED intensity can change for identical growth conditions. Instead, one needs to look at when the longest relaxation time is reached. If the surface is very rough, the relaxation time is short, since the adatoms can quickly find a step edge, hole or island to diffuse to. In turn, an almost complete layer only has a few possible sites for the adatom to move to, resulting in longer relaxation times.

The phase of the RHEED oscillations is a complicated function of multiple diffraction conditions. A change in the incident angle can have a substantial impact on the oscillation phase. It has been reported that additional maxima are observed in the intensity oscillations measured at low incidence angles as well as at higher incidence angles, leading to the belief that this is a diffraction effect [46]. Not only the specular reflection, but also the FWHM of the spots and their separation can show oscillatory behavior during layer-by-layer growth. FWHM oscillations do not show phase dispersion, however. These experimental results give enough reason to assume that the surface roughness is not the only contributing factor to the RHEED intensity.

Changing properties such as the growth temperature or growth rate can change the growth mode from layer-by-layer growth to step-flow growth. It has been reported for homoepitaxial $SrTiO_3$ growth by PLD that using a repetition rate of 5 Hz or less and increasing the annealing temperature gradually will result in a change of the RHEED intensity from an oscillatory behavior to the RHEED intensity sharply recovering after each pulse [14].

2.2 Pulsed Laser Deposition

Pulsed Laser Deposition (PLD) is a technique widely used to deposit high-quality films with a complex composition onto a substrate surface. Using laser ablation, particles from a target material are directed onto a substrate surface, which leads to film growth. PLD is generally used in combination with diffraction techniques such as x-ray diffraction (XRD) or reflection high-energy electron diffraction (RHEED) to monitor the film growth.

2.2.1 Basic principles

In PLD, a pulsed ultraviolet (UV) laser beam is focused on a rotating or scanning target using a mask and lens system, to ensure even ablation of the target surface. The energy of the laser pulse is absorbed by the target surface and the electromagnetic energy is converted into electronic excitations, which results in a rapid heating of the target surface and the formation of a dense layer of vapor in front of the target. Due to the rapid energy absorption, the vapor pressure and target surface temperature increase rapidly, causing ionization and leading to the creation of a plasma plume with the ablated material during this process. During the initial expansion of the plasma plume, additional energy transfer occurs from the laser light to the plasma due to inverse bremsstrahlung heating, leading to kinetic energies of up to 100 eV for the ablated particles. This plume is directed at the sample surface. A higher background pressure will lead to a reduced velocity in the ablated particles due to collisions with the gas molecules. As a result, these background gas parameters can be used to tune down the energy of the particles. However, this can also significantly change the congruence of ablation since atomic species with different masses will scatter at different angles. The substrate is often additionally heated to facilitate the diffusion processes of the deposited particles on the surface.

Even minor changes in any of the deposition parameters, such as deposition rate, number of pulses, substrate temperature, ablation area, target-to-substrate distance, laser fluence (energy per pulse per unit area), and background pressure can alter the growth mode, morphology and composition of a material. The deposition rate per pulse is an especially crucial growth parameter since it directly influences the kinetics of adatoms at the surface [13].

However, a well-defined and clean substrate surface is just as important for depositing high-quality thin films. The process of substrate cleaning is described in Section 3.1.

2.2.2 Chamber setup

All thin film growth experiments were conducted in a pulsed laser deposition chamber. For the ablation, a pulsed KrF excimer laser (Lambda Physik COMPex 201s, Göttingen, Germany), operating at $\lambda = 248$ nm was used. The oxygen pressure in the deposition chamber was kept at a constant value of about 1×10^{-6} Torr with a molecular leak valve. With the help of a focus lens and attenuators, it was possible to adjust the laser fluence by changing the size of the focus spot on the target surface, or the laser pulse energy. The size of the focus spot was kept the same for all experiments. The substrate was annealed with a Nd:YAG heating laser. Its temperature was monitored using an optical pyrometer on the front of the sample. This allowed for a controlled heating ramp during the annealing process. The Nd:YAG laser operates in the near-infrared range at $\lambda = 1064$ nm. Since most oxide substrates are unable to absorb the laser light at this wavelength, a nickel sheet (Nilaco, Tokyo, Japan) that was oxidized in an electric furnace was used as a susceptor to transfer heat to the back of the substrate.

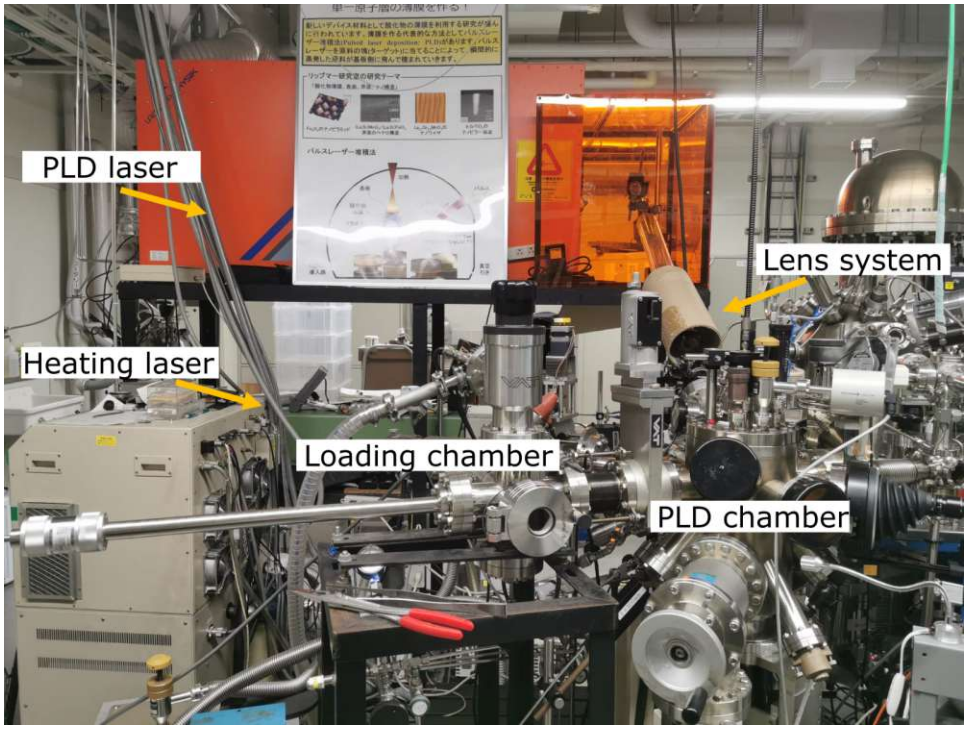

Figure 8: View of the PLD chamber, the PLD laser setup and the heating laser.

2.2.3 Ablation targets

In order to achieve high-quality films, an ablation target with a high optical absorption coefficient for the excimer laser wavelength is needed. However, the composition of the target, impurities and the overall quality of the target can have an influence on the deposition, as unwanted contaminants may alter electronic or crystallographic properties of the film.

All targets were mounted onto a carousel within the PLD chamber and positioned in such a way that the plume was centered upon the sample surface at equal distances.

To remove unwanted contamination from different target ablations or adsorbates from the residual gas, each target was pre-ablated by shooting 5000 pulses at the rotating target surface before film growth. So as to not alter the composition of the targets, approximately the same laser fluence was used for each experiment.

2.3 AFM

Atomic Force Microscopy (AFM) [53] was used to determine the surface morphology of the samples after deposition. AFM is a scanning-probe technique where a sharp tip on a cantilever scans over the sample surface and the force between the sample surface and the tip is detected.

There are different operation modes for measuring with AFM. In contact mode, the tip is moved across the surface while the feedback loop keeps the deflection of the cantilever constant (constant-force mode) by regulating the sample height with a piezoelectric actuator. The cantilever will bend upward or downward depending on the forces acting upon it. When the tip is positioned close to the surface, the force acting on the tip is attractive due to van-der-Waals forces. At smaller distances, the force will be repulsive due to the Pauli exclusion principle. If the elastic constant of the cantilever is known, the force between the tip and the sample surface can be calculated using the cantilever displacement. The cantilever deflection is measured via a laser that reflects from the cantilever onto a segmented photodiode. By scanning the tip across the surface and constantly adjusting the sample height so that a constant contact force (set point) is maintained, the sample height information can be used to construct a three-dimensional topographic image of the surface.

In non-contact mode, the cantilever is driven at its resonant frequency and the force between the tip and the sample surface changes the resonant frequency of the cantilever, the oscillation amplitude, and phase between the drive and optically detected signals. These changes can then be used to maintain a constant distance between the tip and the sample surface by continuously adjusting the sample height with a feedback controller. This mode causes less damage to the sample surface and less contamination of the tip. A Shimadzu SPM-9600 microscope (Shimadzu, Kyoto, Japan) (Figure 9) was used in both contact and non-contact mode for surface morphology analysis. All measurements were taken immediately after taking the sample out of the vacuum chamber to minimize surface contamination from the atmosphere.

Figure 9: Shimadzu SPM-9600 AFM

2.4 Co-Axial Impact Collision Ion Scattering Spectroscopy

Co-axial impact collision ion scattering spectroscopy (CAICISS) is a powerful technique for the analysis of the composition and structure of surfaces. Through an ion source, typically He or Ne ions are accelerated in an electric field with a bias voltage of 2 to 3 kV and passed through a chopper to create pulsed beams which are separated by an interval of 10 – 20 μs. Via an einzel lens, this pulsed ion beam is then focused onto the crystal surface. Most ions are implanted into the crystal, leading to local surface damage, while only a few ions are able to hit the surface atoms and backscatter to the detector at a scattering angle close to 180°.

Since the initial velocity of the ions as well as the flight path length are known, the measured time-of-flight spectrum can be used to calculate the energy loss due to the collision of an ion with a surface atom. Since this energy loss depends on the mass of the target atom, the average ratio of different atomic species on the surface can be determined.

Shadowing of subsurface atoms by surface atoms determines which ions can scatter the incident ions. It is therefore important to consider the geometry of the sample in order to control the influence of the shadow cone, into which no incident ion can reach (see Figure 10).

For cubic perovskites such as $SrTiO_3$, it is common to align the incoming ions along the [111]-direction to make CAICISS sensitive to the surface termination. In this incident direction, the surface atoms shadow the atoms in the center of the cubic unit cell, which means, for example, that if a $SrTiO_3$ crystal is perfectly TiO_2-terminated, the Ti atoms exactly shadow all Sr atoms in the second atomic layer, and thus the Sr signal disappears from the scattering spectrum. For mixed terminations, scattering from both Sr and Ti atoms is possible. By comparing the Sr and Ti peak intensities in a spectrum, the relative surface coverage can be calculated, under the assumption of a pure bulk termination.

A schematic CAICISS measurement comparing two $SrTiO_3$-(001) surfaces with the incoming ions for one surface being aligned along the [111] and for the other along the [001] direction is shown in Figure 10.

In this thesis, CAICISS was used to analyse the surface composition of the samples after deposition in order to determine changes of termination for different targets and growth conditions.

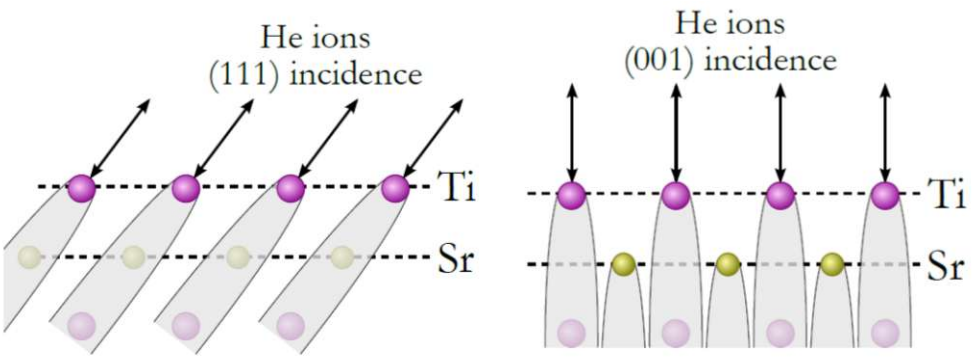

Figure 10: Schematic CAICISS measurement of the $SrTiO_3$-(001) surface along the [111]- and [001]-direction, showing the shadow cones of the surface atoms.

3 Results

3.1 $SrTiO_3$ substrate preparation

The samples used were made from a 15 × 15 × 0.5 mm^3 single-side polished $SrTiO_3$ single crystal purchased from Shinkosha with a (001) surface orientation and a 0.2° miscut. The intentional miscut ensures that the terraces on the surface always have a fixed average width. An AFM image of a commercial $SrTiO_3$-(001) substrate can be seen in Figure 11a. As expected for a substrate miscut of 0.2°, an average terrace width of approximately 120 nm can be observed.

The $SrTiO_3$ 5 mm × 5 mm substrates were put on top of two 0.1 mm thick sheets of nickel for better heat conductance, a 0.3 mm nickel susceptor sheet for absorbing the infrared laser light, and a 11 mm × 11 mm sapphire sheet that functions as a heat insulator but also prevents evaporation of the nickel oxide at high operating temperatures. Before mounting on the sample holder, all substrates were washed to remove contaminants and adsorbates. The individual $SrTiO_3$ pieces were separately put into an ultrasonic acetone bath for 15 min each and dried with nitrogen. Additionally, the 0.1 mm thick nickel sheets were baked to prevent water from condensing onto the surface which is facilitated by acetone. The thin sheets have to be dried more carefully since they are easily bent during the drying process with nitrogen.

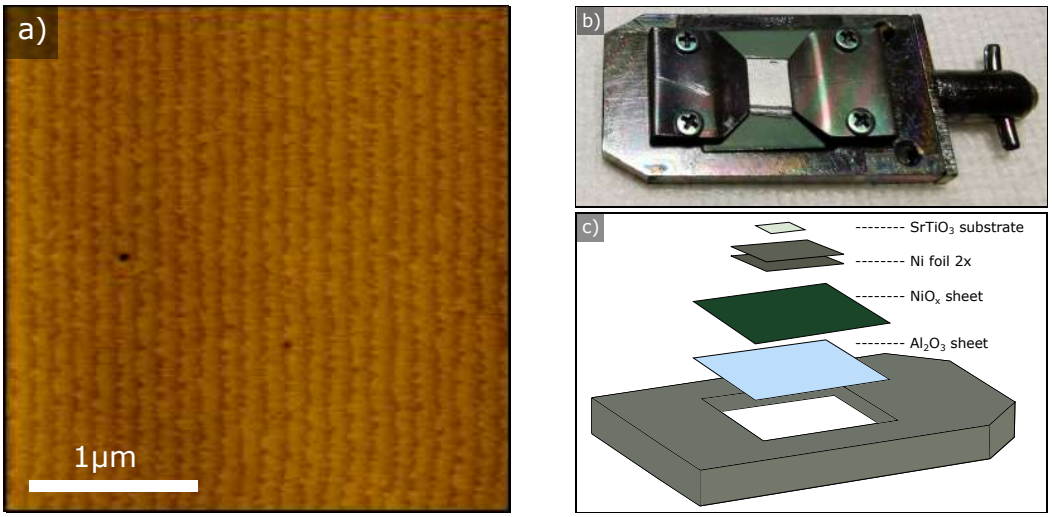

Figure 11: a) AFM topography image of a commercial BHF-etched $SrTiO_3$ step substrate from Shinkosha. b) 5×5 mm^2 sample on top of two 0.1 mm thick sheets of nickel, one 0.3 mm-thick oxidized nickel piece and one piece of sapphire mounted onto the sample holder via clamps. c) Sketch of the sample preparation.

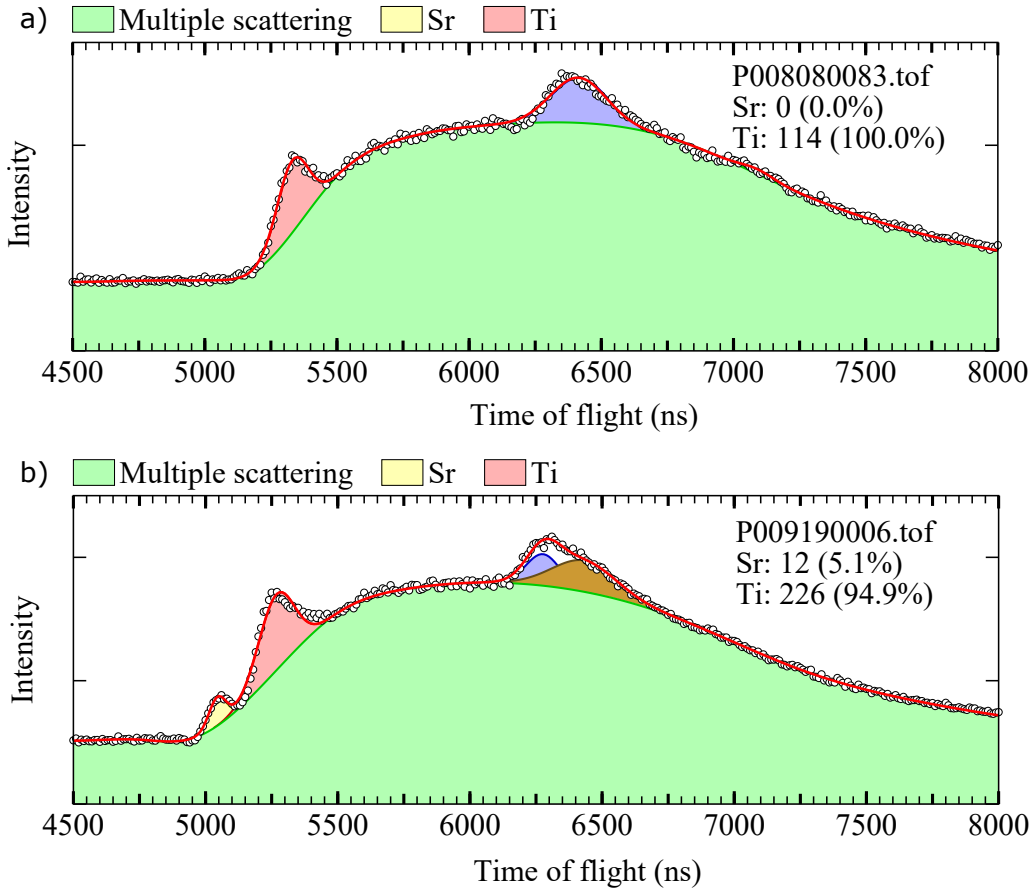

Figure 12: Fitted CAICISS time-of-flight spectrum of a) a commercial $SrTiO_3$-(001) substrate surface b) a prepared substrate surface after annealing to 950 °C for 15 min.

The single crystal substrates were then mounted on sample holders designed for laser heating (sample holder contains a hole that enables heating of the sample via the IR laser) using two clamps before being loaded onto a sample stage in the vacuum chamber. A mounted sample is shown in Figure 11b.

A typical CAICISS measurement of the [111] crystal azimuth of an untreated substrate piece is shown in Figure 12a. The Ti peak is observed, while the Sr peak, which would appear at a flight time of 5100 ns, is not visible in the spectrum, leading to the conclusion that the topmost surface layer is perfectly TiO_2 terminated. *In situ* annealing of the substrate was used to remove adsorbates and to recrystallize the substrate surface from the commercial polishing treatment, to obtain nearly straight and equidistant steps. In all experiments, substrates were annealed to 950 °C in 1×10^{-6} Torr oxygen background pressure prior to deposition. The relatively low oxygen pressure was used to avoid Sr segregation to the surface, which would lead to (2×2) or higher-order surface reconstructions [54].

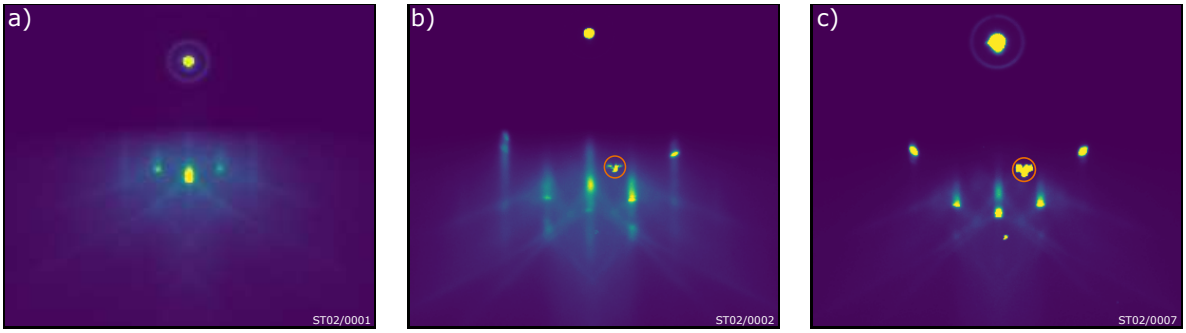

Figure 13: RHEED patterns of $SrTiO_3$ substrate surface of sample surface at a) room temperature, b) at around 600 °C, and c) after 10 min at 900 °C. All three images were take at different glancing angles. The bright feature (indicated by the orange circle) appearing for b) and c) corresponds to a contaminant on the RHEED screen.

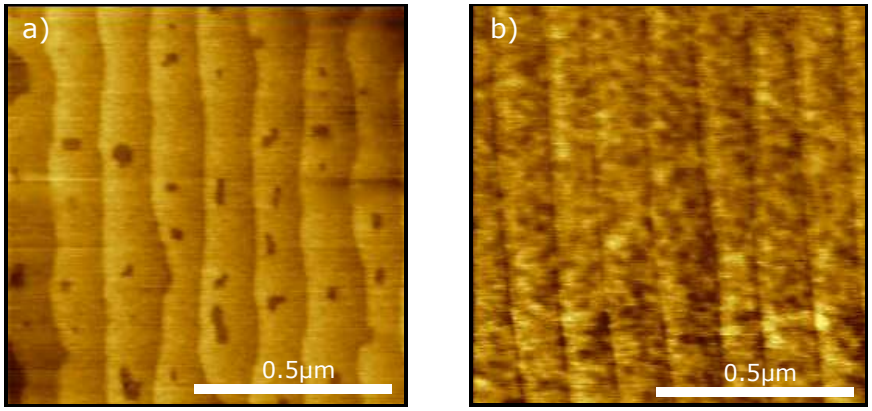

Figure 14: a) AFM topography images of a $SrTiO_3$ substrate where the annealing time was insufficient and b) AFM image of a substrate after annealing at 900 °C for 25 min.

The surface recrystallization process occurs at temperatures of around 500 °C – 600 °C, as can be inferred from RHEED images. The originally sharp diffraction spots at room temperature (Figure 13a) become streaky at 600 °C. However, upon annealing to temperatures close to 1000 °C, the diffraction spots appear sharper again (Figure 13) and a regular step-and-terrace structure is recovered as shown by AFM (Figure 14b). A CAICISS measurement of a sample after the annealing process shows a noticeable Sr peak in the spectrum. This shows that Sr was migrating to the surface layer. Therefore, the surface is no longer purely Ti-terminated.

It was concluded by RHEED pattern observations and AFM image studies that a preparation temperature of 950 °C was sufficient to create straight step edges on the

substrate surface that stay well-ordered after cooling, given that sufficient time was provided. For each experiment the annealing time was set to at least 15 min to prepare the surface. If the annealing time was not sufficient, holes with a depth of a single unit cell were observed in the terraces, as can be seen in Figure 14 a.

3.2 $SrTiO_3$ thin-film growth and RHEED observation

$SrTiO_3$ thin films were grown on $SrTiO_3$-(001) substrates using three different targets: pure $SrTiO_3$, 10% iridium-doped $SrTiO_3$ (Ir:$SrTiO_3$) and 5% platinum-doped $SrTiO_3$ (Pt:$SrTiO_3$). However, since the collected data for using the Pt:$SrTiO_3$ target is insufficient, the RHEED data for these experiments is only found in Appendix A for the sake of completeness. In order to make the experiments more comparable, the same target-to-sample distance was used for all three targets and the laser fluence of 0.25 J/cm^2 was kept at approximately similar values for all depositions. For most experiments the number of pulses was set to 120 which corresponds to a film thickness of about 12 unit cells as measured by a stylus profilometer (Dektak 6M Surface Profiler).

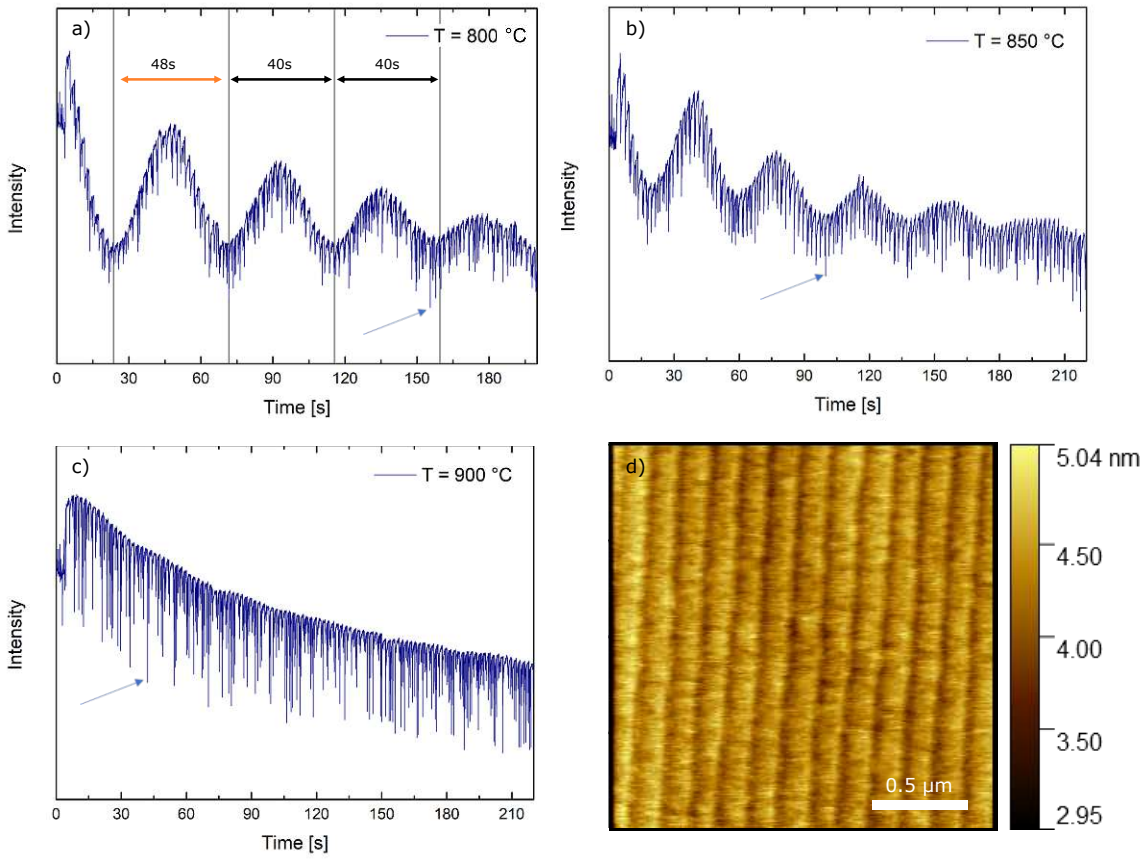

Figure 15: RHEED intensity curve for $SrTiO_3$ homoepitaxial growth with a 0.5 Hz repetition rate at a) 800 °C b) 850 °C and c) 900 °C. The strong spiking in the intensity as indicated by the blue arrows for all three curves is due to a power supply problem. A significant change in the noise level can be observed when comparing these RHEED intensity curves with following ones in this work. d) *Ex-situ* AFM image of the film grown in the step-flow-growth mode.

The nondoped $SrTiO_3$ target and the Ir:$SrTiO_3$ target both showed a similar film thickness after depositing the same number of pulses at approximately the same laser fluence. The Pt:$SrTiO_3$ target showed a lower film thickness by about 20% due to a lower target volume density. This was concluded from the fact that the target was not pressed as well and the observation that the ablated species were also found on the sample holder which is an indicator that the laser pulse was probably absorbed by a porous target surface which changes the shape of the plume and can lead to a wider range of ablation angles during deposition.

Previous works were taken into account for setting up the RHEED system [14]. The oxygen background pressure was set to 1×10^{-6} Torr for all experiments. The growth process was monitored by recording the RHEED intensity during deposition. The average intensity of the specular spot in RHEED was used to create the RHEED intensity curves. A typical RHEED intensity curve for $SrTiO_3$ homoepitaxial growth can be seen in Figure 15b). The repetition rate was set to 0.5 Hz and the RHEED intensity monitored for three different temperatures. Due to problems with the power supply, additional spikes can be seen in the RHEED intensity curve.

The data shows a strictly decaying trend of the overall intensity, however clear oscillations, as expected for layer-by-layer growth, can be observed for temperatures around 800 °C and 850 °C. At temperatures above 900 °C, the behavior changes to pure step-flow-growth, as seen by the characteristic steep drops and recovery of the RHEED intensity, as well as the absence of oscillations. These observations are well in accordance with previous homoepitaxial growth of $SrTiO_3$ [14]. The first oscillation for the deposition at 800 °C has a period of about 48 s, which is longer than for the next two oscillations with around 44 s. This behavior, that the first oscillation period exceeds the following ones by a few seconds, was observed for multiple samples with different deposition parameters. However, the period of the first oscillation was also seen to be shorter for some samples. One possible explanation for this behavior could be the slight Sr segregation on the substrate surface which was shown by CAICISS. On the other hand, the substrate surface and the steady-state film surface have a different roughness which could also contribute to the observed change in the period.

The AFM image of the sample taken after the deposition at 900 °C as seen in Figure 15d) shows smooth equidistant steps across the sample with a step height of 0.8 nm, corresponding to two unit cells of $SrTiO_3$.

After each laser pulse, the intensity of the specular spot will drop instantaneously. This drop was seen to indicate a loss of intensity varying between about 15% to more than

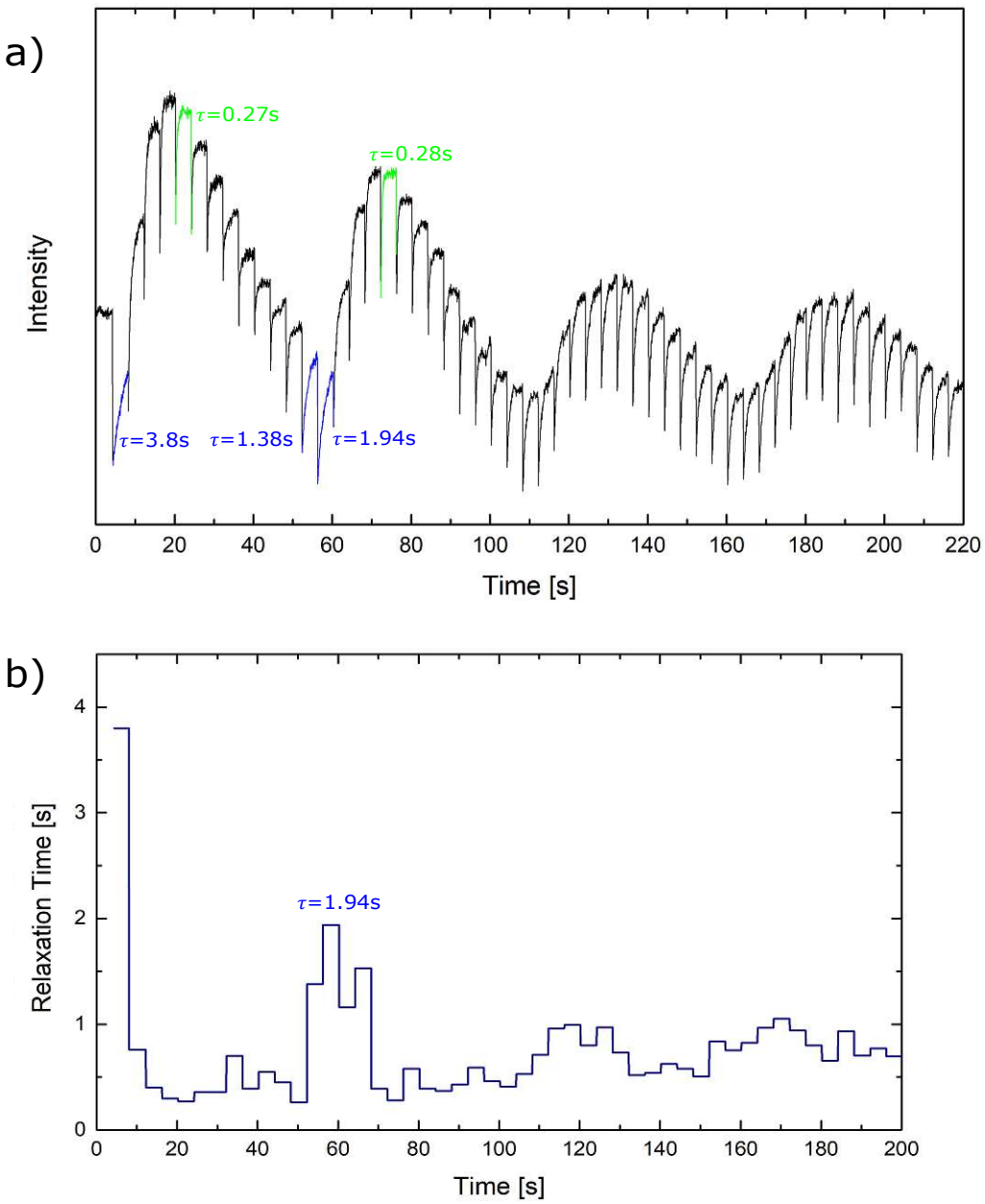

Figure 16: a) RHEED intensity curve for $SrTiO_3$ homoepitaxial growth with a 0.25 Hz repetition rate at 800 °C. The recovery times were calculated for the first two oscillations. b) Corresponding fitted recovery times for every pulse. The complete set of fits for the first two oscillations can be found in Appendix B.

50% of the original steady-state intensity. The intensity recovery time τ was analyzed for layer-by-layer homoepitaxial growth at 800 °C by fitting a single exponential to the individual peaks of the oscillations. The curves were fitted with a single exponential in Origin which uses the Levenberg–Marquardt algorithm. As previously discussed by

Sullivan *et al.* [17], the RHEED intensity is oscillating out of phase with the roughness, as indicated by the shorter recovery time at the oscillation maximum compared to the minimum as seen in Figure 16. The recovery time at the intensity maximum is about 0.28 s whereas at the minimum it is between 1.38 s – 1.94 s. Interestingly, compared to all subsequent pulses, the relaxation time of the first pulse with around 3.8 s is significantly longer. The relaxation time of the second pulse is about 20% of the one of the first pulse. However, there have not been enough samples where it was possible to fit the relaxation time of the first few pulses well enough to make a statement about the reproducibility of this phenomenon.

3.3 Growth-mode study for $SrTiO_3$ and Ir:$SrTiO_3$ thin-films

To compare the deposition of nondoped $SrTiO_3$ with doped $SrTiO_3$, both experiments were conducted on the same day to prevent major changes in the laser fluence or other systematic influences. The samples were prepared the same way by annealing to 950 °C for 15 min in 1×10^{-6} Torr oxygen background pressure and then cooled to the desired deposition temperature. Direct comparisons were made for temperatures 600 °C, 700 °C, 800 °C and 900 °C. The results can be seen in Figure 17.

For temperatures 600 °C and 700 °C, changes in the growth mode for the Ir-doped $SrTiO_3$ deposition can be observed. For both, the 600 °C and 700 °C deposition, the RHEED intensity for Ir:$SrTiO_3$ starts to decrease until the oscillatory behavior is al-

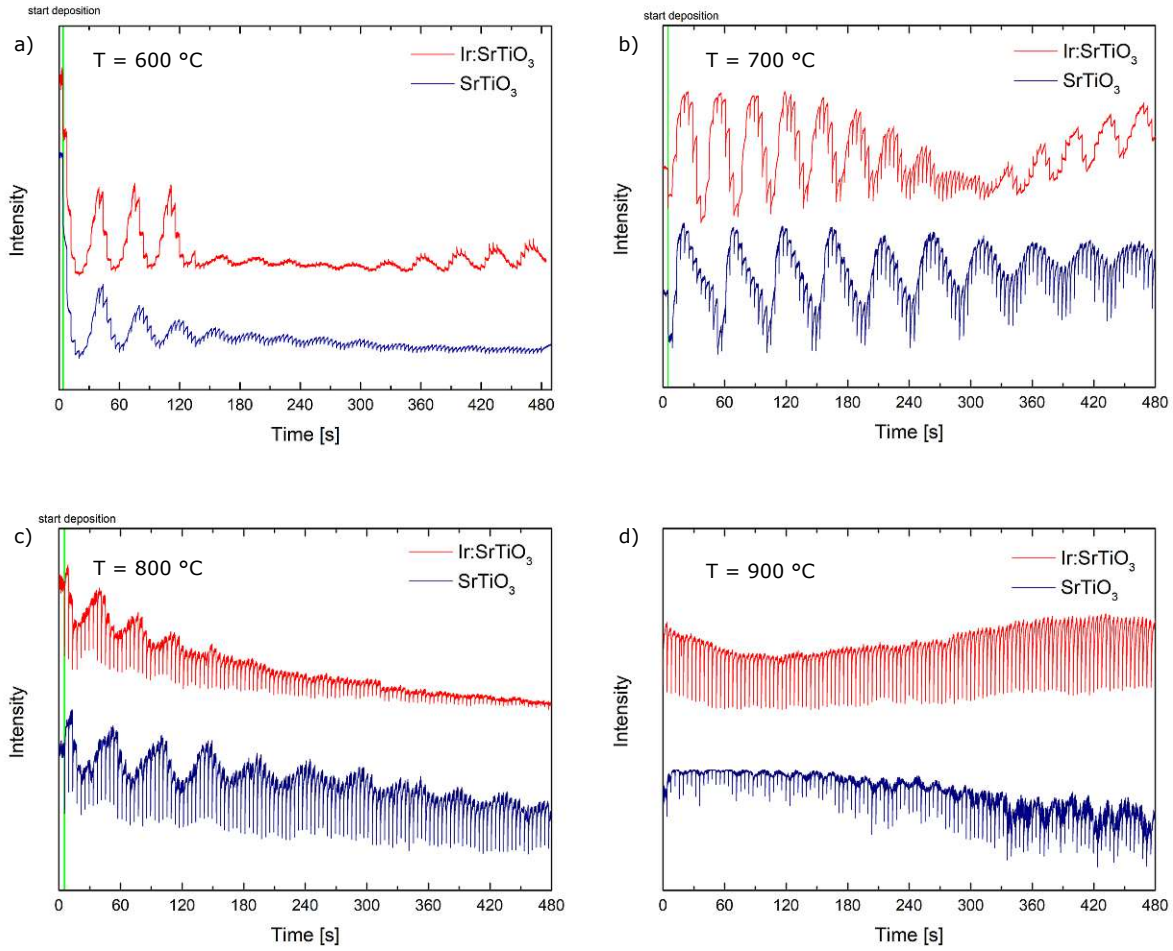

Figure 17: RHEED intensity measurements for 120 pulses of $SrTiO_3$ and Ir:$SrTiO_3$ deposition with a 0.25 Hz repetition rate at a) 600 °C, b) 700 °C, c) 800 °C and d) 900 °C.

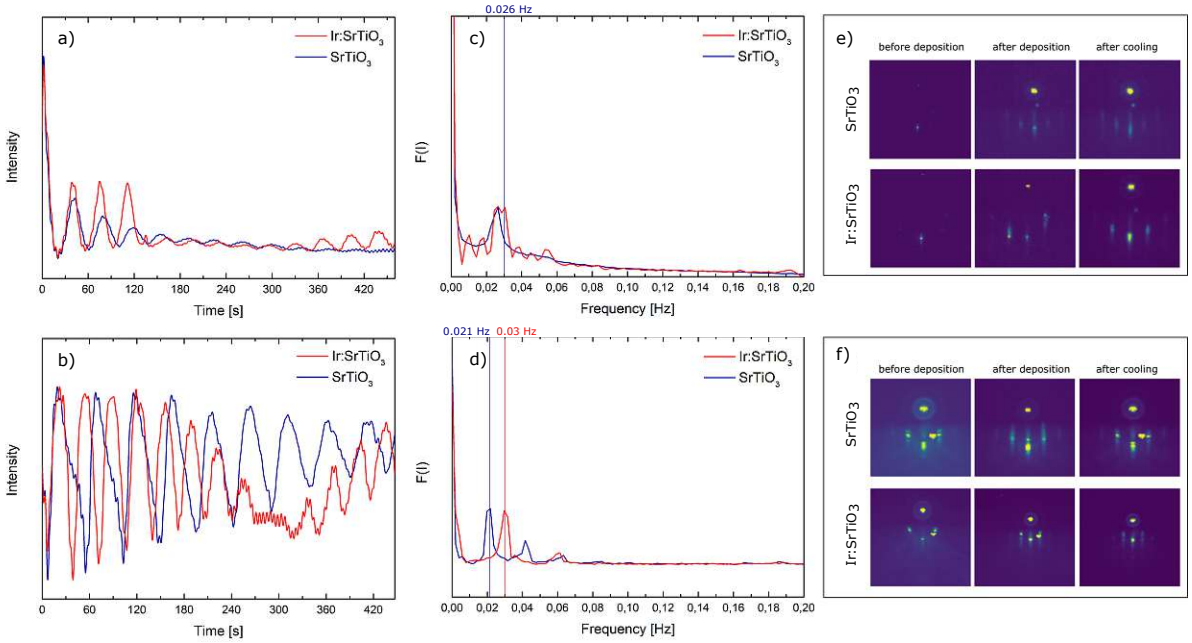

Figure 18: The low-pass filtered RHEED intensity for the results of the temperature series from Figure 17 for temperatures a) 600 °C and b) 700 °C. The oscillations for Ir:$SrTiO_3$ show a lower periodicity compared to $SrTiO_3$ deposition for both temperatures. The Fourier spectrum of the $SrTiO_3$ and Ir:$SrTiO_3$ RHEED intensity curves for c) 600 °C and d) 700 °C. RHEED images before deposition, after deposition and after cooling for e) 600 °C and f) 700 °C. The RHEED pattern for Ir:$SrTiO_3$ after deposition is rotated compared to the the one before deposition, indicating that the RHEED beam was shifted during the deposition.

most non-discernible. For 600 °C, the RHEED intensity suddenly drops at a flank, which has not been reproduced in other experiments. After around 330 s, the intensity starts to increase again, however the shape of the oscillations looks significantly different to the ones at the beginning of the deposition. In addition, the right shoulders of the oscillations appear elongated. However, the recovery of the intensity could also be due the "beating effect" where the number of pulses does not exactly align with the completion of one layer. The sudden change of the intensity, seen at around 135 s at 600 °C when the Ir:$SrTiO_3$ target was used, can be attributed to a shift in the RHEED beam that can be seen in the RHEED pattern in Figure 18e) where the diffraction spots are rotated along the Laue circle. This could also be the reason for the observed change in the oscillatory behavior. In comparison, the nondoped target shows the oscillatory behaviour known from layer-by-layer growth and the RHEED intensity continuously decreases with time. For all four temperatures, the Ir:$SrTiO_3$ deposition shows a shorter periodicity than the nondoped one. This has been confirmed by analyzing and compar-

ing the Fourier spectrum of both RHEED curves for temperatures 600 °C and 700 °C. The results for the Fourier analysis can be seen in Figure 18. 600 °C, the pure $SrTiO_3$ deposition only shows one distinct peak around 0.026 Hz, corresponding to a period of about 38.2 s. In comparison, the main contribution of the RHEED Fourier spectrum of the Ir:$SrTiO_3$ deposition at around 0.03 Hz shows a double peak with the 0.026 Hz peak, corresponding to a period of about 33.3 s. A stronger change is observed at 700 °C where the main peak for the Ir:$SrTiO_3$ spectrum is centered around 0.03 Hz whereas the $SrTiO_3$ peak is present at around 0.021 Hz, corresponding to a period of 47.6 s. The effect that the periodicity of the RHEED oscillations for $SrTiO_3$-(001) homoepitaxy can increase with higher temperature, as seen here in the case of the $SrTiO_3$ deposition, has already been noted by Lee *et al.* [55]. The authors claim that this might be a sign that the periodic oscillations are not purely due to layer-by-layer growth, however, an exact explanation for this behavior has not been given. Evaporation might also be a reason for this observation. In comparison, the periodicity of Ir:$SrTiO_3$ growth decreased at 700 °C and only at 800 °C there is an increase of the period for the oscillations to about 37.4 s.

More importantly, the change in the growth mode to step-flow growth can be observed earlier in the RHEED data for the Ir:$SrTiO_3$ deposition for both, the 800 °C and 900 °C measurements. 800 °C the growth mode for Ir:$SrTiO_3$ changes from oscillations to pure step-flow growth, whereas the non-doped $SrTiO_3$ RHEED data still shows some oscillatory behavior towards the end of the deposition period. 900 °C, already at the start of the deposition, the growth mode for Ir:$SrTiO_3$ is strict step-flow growth. The non-doped $SrTiO_3$ deposition also shows predominantly step-flow growth behavior, but there is still some oscillatory behavior observed.

These results suggest that a layer during layer-by-layer growth is completed faster when using the Ir:$SrTiO_3$ target. However, the occurrence of that behavior could depend on multiple factors.

Experiments conducted on the $SrTiO_3$-(110) surface have shown that different surface reconstructions can lead to different sticking coefficients, thus affecting the film stoichiometry and changing the ability of the surface to integrate the ablated species into the surface [56]. RHEED patterns for the results of the temperature series for 600 °C and 700 °C for both $SrTiO_3$ and Ir:$SrTiO_3$ deposition can be seen in Figure 18e,f). The RHEED patterns after deposition for both targets do not show a substantial change, such as the appearance of additional spots compared to the image taken before deposition. This suggests, that the deposition does not lead to different surface

reconstructions which can alter the growth mode.
A similar change of the growth mode for Ir:$SrTiO_3$ was observed when depositing 120 pulses on a $SrTiO_3$ substrate using a repetition rate of 0.5 Hz as seen in Figure 19a). However, unlike the deposition at 0.25 Hz, the periodicity is only slightly altered over time, as seen by the broadened peak in the Fourier spectrum (Figure 19b). Previous works on the $SrTiO_3$-(001) surface have demonstrated, that the laser fluence plays an important role in the Sr/Ti ratio of the grown $SrTiO_3$ film since the fluence not only determines the plume propagation dynamics but also the incongruence of the ablation [57, 58]. While the exact mechanisms for the fluence-dependent Sr/Ti-ratio are still discussed in the literature, lower laser fluence has been shown to produce more Sr-rich films [56]. One explanation for this behavior is that low ablation fluence leads to the plume being slowed down before reaching the surface, thus the material has to diffuse into the background gas to reach the substrate, which can lead to highly non-stoichiometric growth due to collisions [57]. However, since the background pressure was set to 1×10^{-6} Torr, this effect is expected to be rather negligible. This loss of Ti-species can be compensated for by reducing the substrate-to-target distance. In addition, old excimer gas is known to lead to more Sr-rich films [56] even when the discharge voltage is unchanged. The origin of this effect has not yet been determined. Due to the usage of low laser fluence for all experiments, the film is expected to grow Sr-rich. It should be noted that approximately 2 weeks passed between the temperature series measurements and the 0.5 Hz repetition rate experiment. In addition, the excimer gas was refilled between the experiments for the 600 °C and 700 °C comparison. Therefore, it can be concluded that the additional Sr-rich growth expected from using old excimer gas, does not play a significant role for the change in the growth mode for Ir:$SrTiO_3$.

Due to the shift in periodicity for 600 °C and 700 °C, the surfaces of the Ir:$SrTiO_3$ doped samples were analysed with CAICISS to determine whether a switch in the surface termination occurred. While it is noticeable that the Sr concentration is reduced in the spectrum for the deposition at 0.25 Hz (Figure 19 c) compared to the 0.5 Hz deposition (Figure 19 d), this could be the result of the Sr peak for the fit not being perfectly aligned, thus leading to a large error in the resulting concentration. In addition, the multiple scattering background is significantly larger in the spectrum, which suggests lower surface crystallinity and could lead to the broadening of the peaks. For the 0.5 Hz deposition, the Sr coverage lies below 20% but is slightly higher than the prepared substrate (Figure 12b). It should be noted, that only one reference sample

was used for comparison. The sample for 700 °C (Figure 20) still showed a dominant Ti termination suggesting that the concentration of Sr-terminated surface domains still remains comparable low, indicating that the Sr/Ti ratio in the film is not significantly changed. Therefore, it can be assumed that this is not the major cause for the growth mode change.

Another important factor to consider during deposition is the ablation target itself, as explained in Section 2.2.3. Contaminants or uneven ablation of the target material can lead to changes in the surface morphology, thus leading to different plume compositions. In addition, the amount of material ablated by each laser pulse is also determined by the absorption rate at the wavelength of the laser. This needs to be especially considered when using two different target materials. The Ir:$SrTiO_3$ showed a darker color than the $SrTiO_3$ target due to oxygen vacancies which are formed when ablating at low oxygen background pressures. However, a difference in absorption rate at the laser wavelength is unknown. The ablation behavior of the pressed Ir:$SrTiO_3$ target could also be different due to a lower target volume density. For PLD, the laser fluence needs

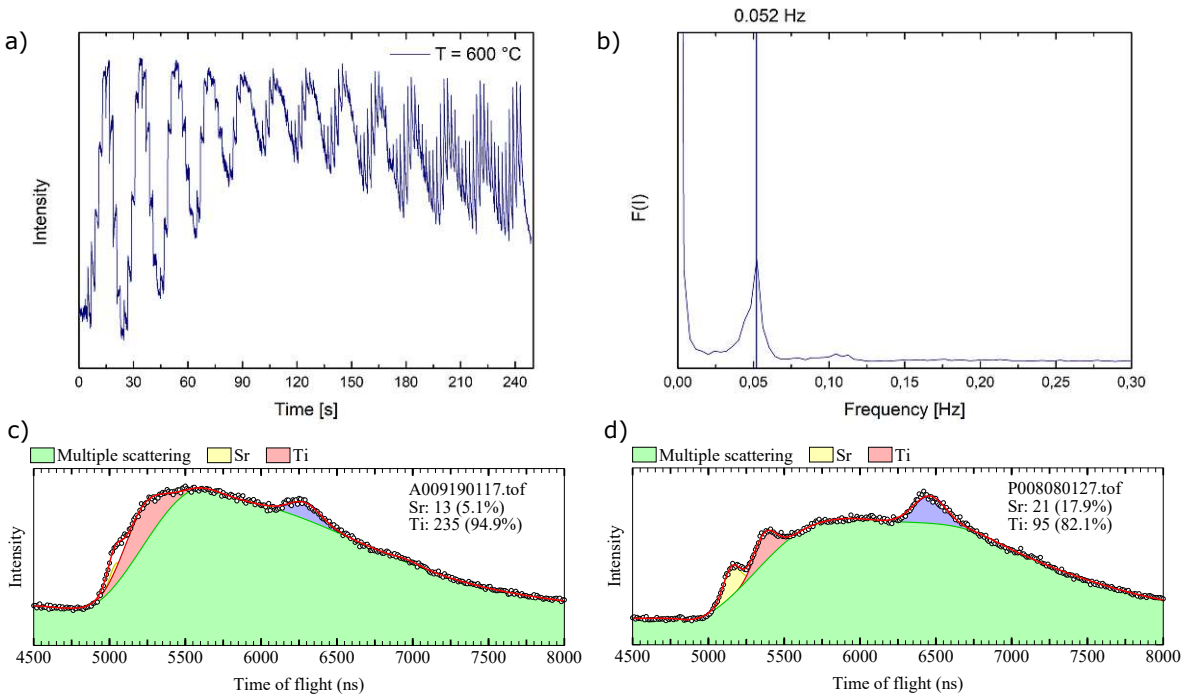

Figure 19: a) RHEED intensity curve when depositing 120 pulses of Ir:$SrTiO_3$ with a 0.5 Hz repetition rate. b) Fourier spectrum for the low-frequency regime for the RHEED intensity in c) CAICISS measurement after depositing 120 pulses of Ir:$SrTiO_3$ at 600 °C with a repetition rate of c) 0.25 Hz (temperature series) and d) 0.5 Hz onto the sample.

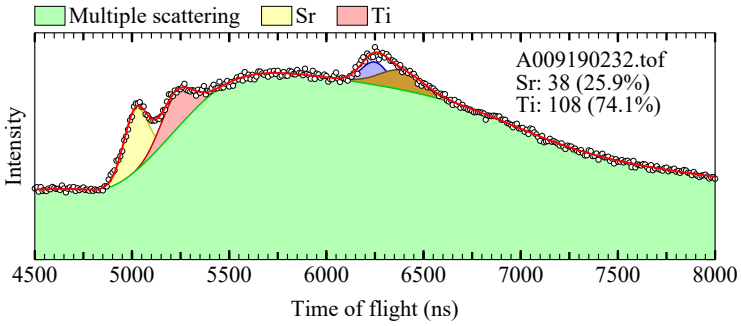

Figure 20: CAICISS measurement after 120 pulses at 0.25 Hz of Ir:$SrTiO_3$ at 700 °C were deposited onto the sample.

to be sufficiently above the ablation threshold fluence to ensure near-stoichiometric ablation. For all experiments in this thesis, the $SrTiO_3$ target used is a single crystal whereas the Ir:$SrTiO_3$ target is a polycrystal ceramic which could result in different ablation thresholds. In addition, the targets were never ground between experiments, which could have resulted in changes in the stoichiometry or roughness of the target surfaces.

In conclusion, it was shown that thin film growth on a $SrTiO_3$ substrate using a Ir:$SrTiO_3$ target leads to short periodicity in the RHEED intensity oscillations in comparison to pure $SrTiO_3$ growth for all temperatures used in this thesis. In addition, step-flow growth also occurs at lower temperatures (at 800 °C) for Ir:$SrTiO_3$ depositions compared to 900 °C for pure $SrTiO_3$. A change in the growth mode for 600 °C and 700 °C is also observed. The most likely cause for the periodicity difference is a slightly different ablation rate from the polycrystalline Ir:$SrTiO_3$ target. As for the growth mode differences, a number of possible mechanisms were considered but since no significant differences in the surface morphology or termination were found, a difference in the effective surface migration rate of adatoms remains the best explanation. Specifically, comparison of RHEED images before and after deposition suggest that a change in the surface reconstruction which can lead to a different sticking coefficient thus impacting the flux of diffusing particles, does not occur. However, the differences in the growth modes of the non-doped and Ir-doped films were minor. It should also be noted, that the effective Ir concentration of the films was not verified using a surface composition technique such as quantitative x-ray photoelectron spectroscopy (XPS). Diffusion of the Ir species might be the reason why only minor changes were observed. For future experiments, these techniques should be conducted as well in order to determine the effect of the Ir concentration of the films on the growth modes.

3.4 One pulse Comparison

As discussed in Section 2.1.2, the RHEED intensity is modulated by each laser pulse during deposition. As soon as the ablated material reaches the surface, the RHEED intensity drops due to adatom cluster nucleation and the roughening of the surface. Surface migration leads to a (partial) recovery of the system after a given time. The diffusion process is heavily influenced by temperature, due to the rate equation having an exponential dependence on the temperature. At higher temperatures, the RHEED intensity recovers considerably faster. It has been shown that the nucleation on the surface upon deposition can be observed via *in-situ* scanning tunnelling microscopy. In addition, the oxygen pressure also affects the diffusivity. It has been shown that the oxygen pressure can heavily influence the surface morphology of metal-oxide thin films [59]. Low oxygen pressures have shown to lead to a higher diffusion of the ablated species on the surface. A correlation between the oxygen chemical potential, which is determined by the temperature and the oxygen background pressure, and the surface morphology for metal oxides has been observed [59]. The authors suggest, that the chemical potential changes the oxygen stoichiometry of the diffusing species, thus changing their ability to diffuse on the surface. The influence of the scattering of the plume species with the background gas on the diffusivity, which has been previously suggested [15], was ruled out.

In this thesis, the relaxation behavior of the RHEED intensity during deposition on $SrTiO_3$ at 800 °C, depending on the target material used, has been studied. As seen in Section 3.2, the recovery time depends heavily on the coverage of the surface, thus can be used to indicate the completion of a layer during film growth. To simplify the comparison between different targets, the behavior of the RHEED intensity for the very first pulse onto the prepared sample surface was studied. The immediate effect of Ir:$SrTiO_3$ on homoepitaxial growth was investigated by conducting one-pulse experiments at 800 °C for both $SrTiO_3$ and Ir:$SrTiO_3$ targets. The results for all pulses can be seen in Figure 21. Since it is not clear whether the Ir as a deposited species or as an incorporated species has an effect on the growth dynamics, one pulse of Ir:$SrTiO_3$ was shot on a prepared $SrTiO_3$ surface with a prior 5 pulse deposition of Ir:$SrTiO_3$ (Figure 21b), one on a prepared $SrTiO_3$ surface without any prior deposition (Figure 21c) and another one onto a surface where 5.5 ML of Ir:$SrTiO_3$ were previously deposited and then annealed to 950 °C for 10 min (Figure 21d). It has to be noted that the experiments for the non-doped $SrTiO_3$ pulse in Figure 21a) and the Ir:$SrTiO_3$ pulse in Figure 21b) were conducted on different days as opposed to the Ir:$SrTiO_3$ depositions

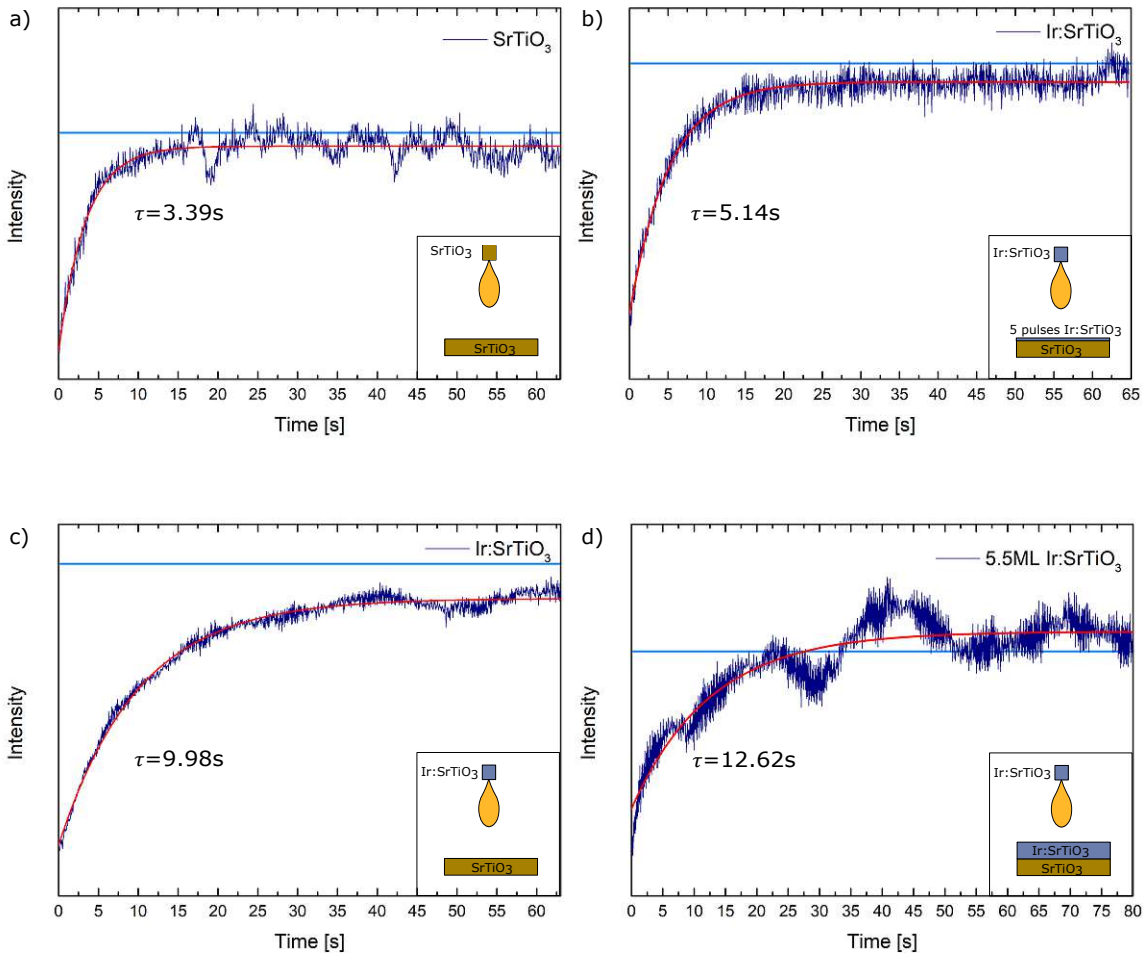

Figure 21: Exponentially fitted relaxation time for: a) one pulse of $SrTiO_3$ on a prepared $SrTiO_3$ surface, b) one pulse of Ir:$SrTiO_3$ deposited on $SrTiO_3$ with a prior deposition of 5 pulses, c) one pulse of Ir:$SrTiO_3$ on a prepared $SrTiO_3$ surface without prior deposition and d) one pulse of Ir:$SrTiO_3$ on a prepared $SrTiO_3$ surface after depositing 5.5 ML of Ir:$SrTiO_3$, at 800 °C. Experiments for c,d) were conducted on the same day. The temperature for all depositions was 800 °C. The average steady-state value for the intensity is indicated with I_0.

in Figure 21c,d). The measurements show that non-doped $SrTiO_3$ has the shortest relaxation time with 3.39 s. In contrast, the Ir:$SrTiO_3$ depositions show longer relaxation times ranging from about 5.14 s for prior deposition of 5 pulses to about 10 s without prior deposition and about 12.6 s for the surface with 5.5 ML of deposited Ir:$SrTiO_3$. Within 20 s, the $SrTiO_3$ RHEED intensity almost recovers to the original value of the intensity I_0 which was taken as the average steady state intensity before deposition. In comparison, the RHEED intensity for Ir:$SrTiO_3$ deposited on the prepared surface is only partially recovered and even after 65 s the original value is not reached. Due to

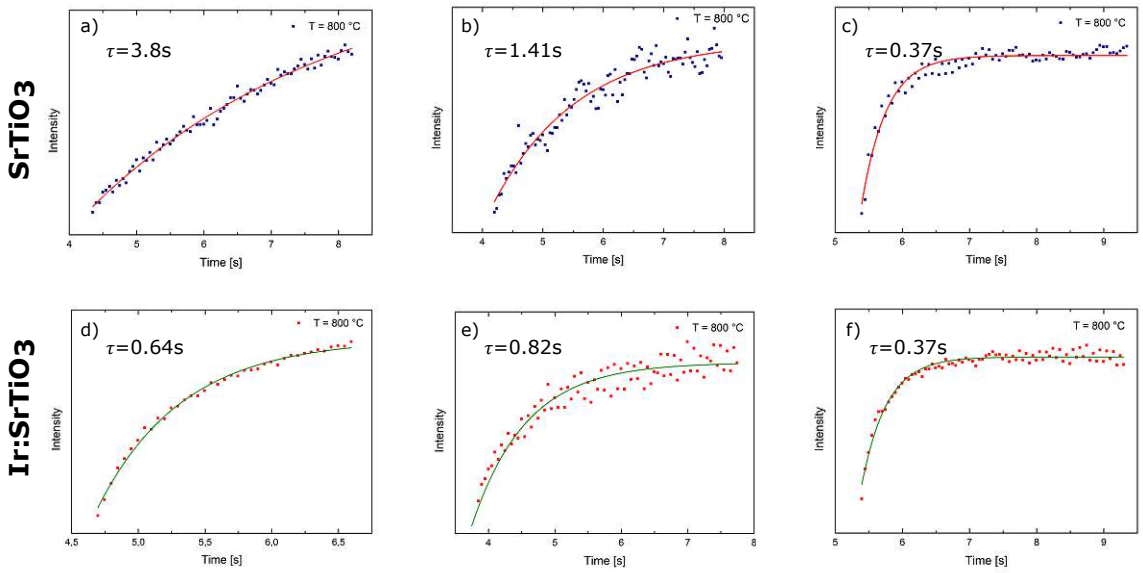

Figure 22: Exponentially fitted relaxation time for: a-c) one pulse of $SrTiO_3$ deposited on a prepared $SrTiO_3$ surface, d-f) one pulse of Ir:$SrTiO_3$ deposited on a prepared $SrTiO_3$ surface.

some oscillations in the intensity of Ir:$SrTiO_3$ on the 5.5ML-Ir:$SrTiO_3$ surface, it is not clear to what extend the noise contributes to the recovery above the steady-state value. These preliminary results would suggest that pure $SrTiO_3$ deposition has a lower relaxation time than Ir:$SrTiO_3$ regardless of prior Ir:$SrTiO_3$ deposition. However, at this point the question how reproducible the relaxation times across different experiments conducted under the assumed "equivalent" circumstances are, has to be asked. For that reason, the first pulses for film growth experiments at 800 °C using non-doped $SrTiO_3$ and Ir:$SrTiO_3$ targets were fitted to compare the relaxation times. The fitted curves can be seen in Figure 22. For non-doped $SrTiO_3$, the relaxation times of the first pulses range from 0.37 s to 3.8 s. In comparison, the relaxation times found for the first pulse from film growth for Ir:$SrTiO_3$ were all about 10 times shorter than the ones for the one-pulse experiments. This suggests that the values from the one-pulse experiments for Ir:$SrTiO_3$ still lie within the error range of the $SrTiO_3$ one. In addition, for $SrTiO_3$ the relaxation time of the second pulse was seen to range from being about 20% shorter to being 20% longer than the one from the first pulse.

One possible explanation for this difference in the relaxation times is that the surface morphology plays a much more significant role in the recovery of the RHEED intensity for the first pulse than the presence of Ir on the surface. Already in Figure 16, a large

difference in the recovery time between the first pulse and all subsequent pulses for non-doped $SrTiO_3$ thin film growth was noticed. For that reason, the RHEED patterns for the non-doped $SrTiO_3$ and Ir:$SrTiO_3$ on the $SrTiO_3$ one-pulse experiments were analyzed (Figure 23). The RHEED pattern after on pulse of Ir:$SrTiO_3$ shows a periodic feature corresponding to a real-space distance of approximately 1.36 nm. It is possible that this characteristic of the substrate's surface morphology may have contributed to a lower surface mobility of the adatoms, thus leading to a longer relaxation time and the RHEED intensity not recovering to its original value.
Therefore, it can be concluded that the conditions under which the experiments in this thesis were conducted are insufficient to compare the effect of Ir on $SrTiO_3$ homoepitaxial growth. A tight control of the surface morphology is crucial for comparing the relaxation times for the first pulse using different target materials.

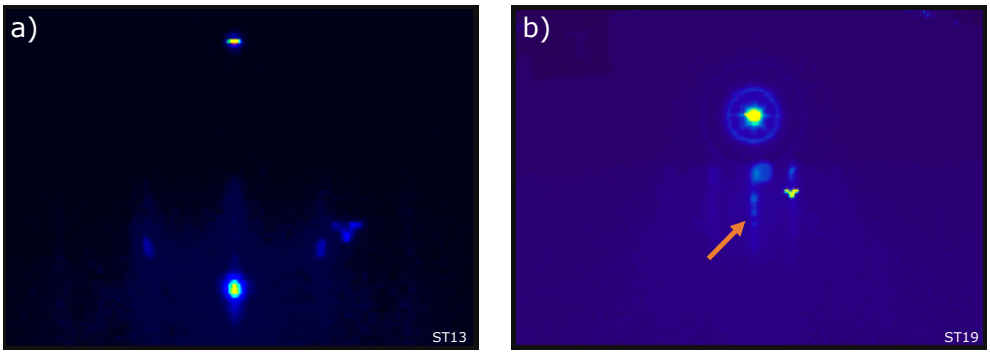

Figure 23: RHEED image after deposition of a) one pulse of $SrTiO_3$ deposited on a prepared $SrTiO_3$ surface, b) one pulse of Ir:$SrTiO_3$ deposited on a prepared $SrTiO_3$ surface. A periodic structure is visible in the RHEED pattern for Ir:$SrTiO_3$ as indicated by the orange arrow.

3.5 Iridium nanopillar formation

The growth of various noble metals on metal oxide surfaces has been a widely studied topic for many years. Especially the formation of noble-metals clusters upon deposition has been intensely studied for the purpose of catalysis [60]. The formation of embedded nanoscale particles in a metal oxide material such as the growth of self-organized Ir nanopillars in a $SrTiO_3$ matrix for photo-electrochemical water splitting electrodes have been reported [61]. Segregation of Ir in Ir-doped $SrTiO_3$ film upon deposition resulting in Ir-clusters of macroscopic size as well as on unit cell scale has been observed for a 5% doping level [62]. It is suggested that the precipitation occurs already at the initial substrate interface during growth leading to the formation of Ir rods in the film growth direction. Due to the robust nature of the embedded nano-structure and the relatively simple method to create them since their growth occurs self-organized, these Ir nanopillars are promising candidates to improve the lifetime of photocatalysts.

In this thesis, the circumstances under which segregation of Ir-clusters occurs and how they influence the growth mode of Ir:$SrTiO_3$ compared to pure $SrTiO_3$ film growth was investigated. According to Lee *et al.* [62] the oxygen pressure is a significant parameter for noble-metal dopants. At high pressures in the range of 1×10^{-1} Torr, Ir can form IrO_3 which can lead to evaporation of the Ir during film growth. Low pressures tend to prevent evaporation and in the range of 10^{-6} Torr, Ir:$SrTiO_3$ films were reported to grow homogeneously. For that reason, the pressure for all experiments in this thesis were fixed at 10^{-6} Torr. Similar to the growth parameters used for the experiments here, Lee *et al.* prepared the $SrTiO_3$ surfaces by annealing at 900 °C for 10 min to obtain flat step-and-terrace surfaces before deposition. The laser fluence of their KrF excimer laser was set to 0.64 J/cm^2 which is higher than the laser fluence used in this thesis, however it is still in the Sr-rich ablation regime.

For all prior Ir:$SrTiO_3$ depositions using 120 pulses and a repetition rate of 0.25 Hz (see Section 3.3), no clustering was visible via AFM. The first occurrence of nano-scale clusters was observed after depositing 120 pulses of Ir:$SrTiO_3$ at a 0.5 Hz repetition rate for each temperature starting from 600 °C to 950 °C in steps of 50 °C and preparing the surface by annealing to 900 °C for 10 min between depositions. Before cooling, the surface was again prepared at 950 °C. The resulting *ex-situ* AFM images can be seen in Figure 24. The images reveal multiple nano-scale clusters with cross-sections ranging from 60 nm to 130 nm. The cluster density is around 15 clusters per 1 μm^2. Islands with a height of 1 u.c. along the terraces are also discernible. RHEED images after deposition reveal additional spots associated with 3D growth. Since no chemical

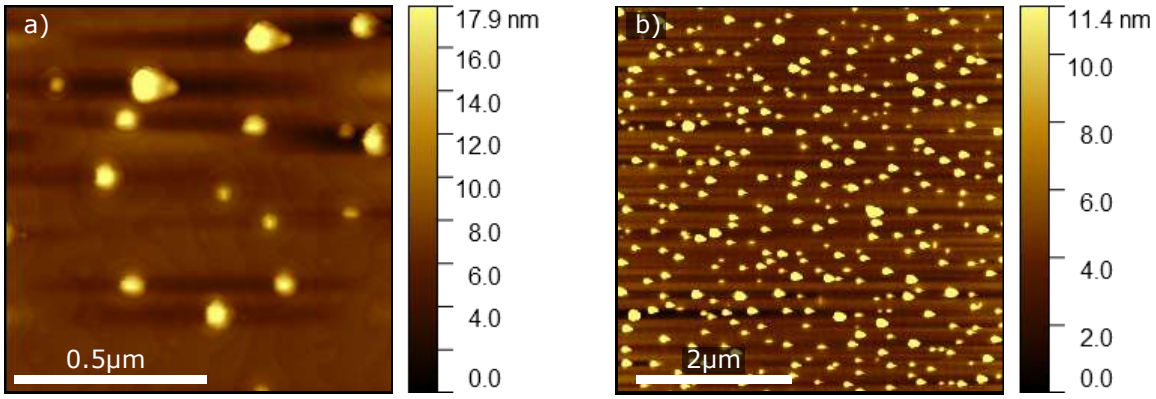

Figure 24: AFM images of a $SrTiO_3$ sample after depositing 120 pulses of Ir:$SrTiO_3$ with a 0.5 Hz repetition rate at temperatures 600 °C up to 950 °C for 50 °C steps respectively. The sample was annealed to 950 °C for 10 min before cooling. AFM of an area of a a) 1×1 μm^2 and b) 5×5 μm^2 area.

composition techniques such as XPS were used to identify the elemental composition of these clusters, it is not possible to unambiguously attribute the clusters to Ir nanopillars. However, the AFM images show accumulated material around the clusters which are situated along the terraces. As a result, the terrace shape has changed from straight steps into a wave-like shape around the clusters. This behavior is similar to the formation of $SrTiO_3$ cones around the Ir pillars reported by Kawasaki *et al.* [61]. These authors also reported that the crystal quality of the film was very high and suggest that the Ir segregation and fast diffusion are responsible for suppressing the formation of defects.

Due to the AFM only being taken after all depositions have been made and the surface having been annealed to 950 °C prior to cooling, it is unclear at which temperature the potential precipitation of Ir occurred and how the state of the surface was affected after deposition. In addition, it should be noted that the laser fluence was lower (0.19 J/cm^2) than the value used in all the other experiments (0.25 J/cm^2).

When depositing a similar number of pulses (due to refilling of the laser gas and slightly lower laser fluence for the previous experiment, the number of pulses was lowered from 960 to a total of 720) but with a deposition rate of 0.25 Hz and only at 600 °C without annealing to 950 °C afterwards, no visible clusters were discernible via AFM (Figure 25a). Due to the exponential dependence, temperature should be the dominant factor for precipitation of Ir.

However, the lower repetition rate most likely also played a role in the absence of visible clusters. This is demonstrated when using a repetition rate of 1 Hz which leads again

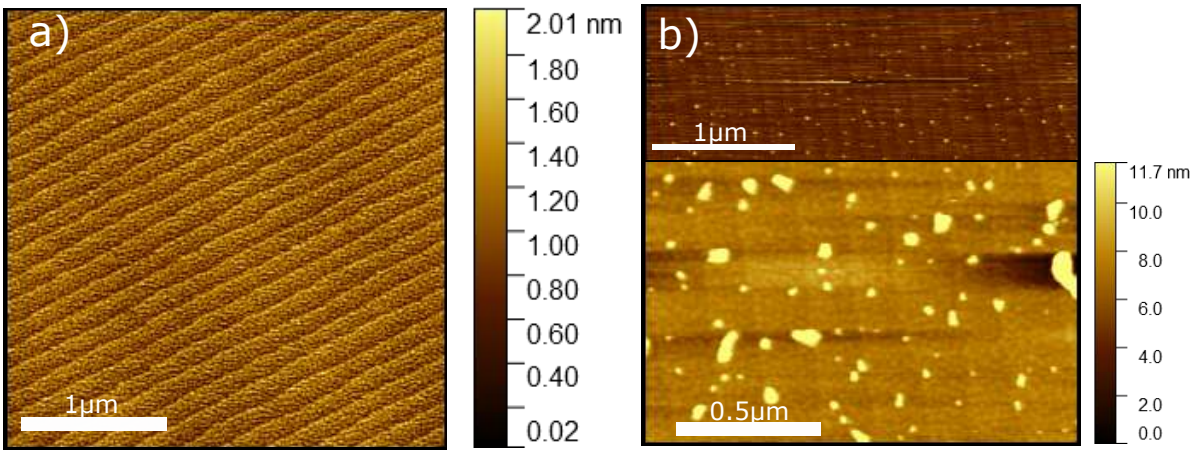

Figure 25: a) AFM image of a $SrTiO_3$ sample after depositing 720 pulses of Ir:$SrTiO_3$ with a 0.25 Hz repetition rate at 600 °C. No clusters are visible on the surface. b) AFM images of a $SrTiO_3$ sample after depositing 720 pulses of Ir:$SrTiO_3$ with a 1 Hz repetition rate at 600 °C. Nano-scale clustering occured on the surface.

to cluster formation at 600 °C as seen by the AFM images in Figure 25b). Compared to the previous surface with clusters (Figure 24), the terraces are still aligned in a straight fashion and have not changed into the corrugated structure as seen before. In addition, the cluster density is higher and the cluster size smaller compared to the Ir precipitation of the previous experiment. This can be explained by the decreased mobility of the surface species at lower temperatures, thus making it more difficult to find existing clusters to attach onto.

It was attempted to study the cluster formation for the repetition rates of 0.5 Hz and 1 Hz but only depositing 120 pulses onto each sample. Neither at 700 °C nor at 800 °C cluster formation was observed. RHEED data for a 0.5 Hz repetition rate shows clear oscillations for about 16 u.c. indicating layer-by-layer growth. RHEED data for the 1 Hz repetition rate has poor quality and is thus insufficient for analysis. Lee *et al.* [62] reported the occurrence of a change of the surface termination after the growth of around 10 u.c. of Ir:$SrTiO_3$ at 700 °C. This surface termination switch was not observed for 700 °C and a 1 Hz repetition rate. In addition, they report step-and-terrace surfaces for all depositions at 1×10^{-6} Torr, which is in accordance to the results presented here. However, they still showed that Ir segregation occurred already during the growth of the first monolayer by using XPS and high-angle annular dark-field scanning transmission electron microscopy (HAADF-STEM) measurements.

While the results in Figure 24 and Figure 25 show similarities with the nano pillar structures reported in the literature [62], it is unclear whether the clusters are generated via

segregation of Ir. Annealing the surface to 950 °C after deposition does not only lead to larger clusters, but also to a change in the step-and-terrace structure which could be explained by the temperature-driven increase in the migration length of the surface species. Instead of straight terraces, material strongly accumulates close to the clusters, which strongly hints at the nano pillar formation reported by Lippmaa *et al.* [5] via HAADF-STEM where a $SrTiO_3$ collar surrounds the Ir nano pillar. In order to reveal whether Ir is still present in the film or diffusion into the bulk occurred and whether Ir segregation occurred, measurements using XPS or HAADF-STEM would be needed since the cluster size (if clusters are present) seems to be below the AFM resolution limit. In addition, more measurements regarding the formation of surface clustering for Ir:$SrTiO_3$ for the low pressure regime are still needed. According to Ref. [61], evaporation of Ir should not occur for the pressure range of 10^{-6} Torr. The data presented in this thesis suggests, that either bulk diffusion of Ir occurs — hindering surface clustering — or the migration length of the Ir species is insufficient, thus the cluster sizes are below the spatial resolution for AFM. More experiments are needed to determine the surface clustering regime and measurements using surface- and bulk-composition analysis techniques are required to accurately determine the origin of the clusters and whether they are the nano pillars reported in the literature.

4 Conclusion

In this thesis, the effect of noble metals on $SrTiO_3$ thin film growth via pulsed laser deposition (PLD) was investigated by mainly using Ir as the focus of study. *In situ* reflection high-energy electron diffraction (RHEED) was used to monitor the growth modes for thin films of both non-doped $SrTiO_3$ and Ir-doped $SrTiO_3$. It was attempted to minimize any differences in the deposition parameters in order to make the effect of both targets on the film growth comparable.

The results show that there is a difference in the growth mode for all temperatures between 600 °C and 900 °C. Analyzing the periodicity of the RHEED intensity oscillations before step-flow growth sets in reveal that in all cases the periodicity for Ir-doped $SrTiO_3$ is shorter than for non-doped $SrTiO_3$ and that a change in the growth mode occurs for temperature 600 °C and 700 °C which was not observed for non-doped $SrTiO_3$. In addition, the transition to pure step-flow growth occurs earlier (i.e., at 900 °C) for Ir-doped $SrTiO_3$. The origin of the change in the growth mode was investigated by comparing the RHEED pattern before and after deposition and determining the surface termination using co-axial impact collision ion scattering spectroscopy (CAICISS). Since neither a change in the surface structure via RHEED nor a significant difference in the surface termination was measured, a difference in the effective surface migration rate of adatoms remains the best explanation. However, even though low pressures of 10^{-6} Torr were used to prevent the evaporation of Ir species, the actual concentration of the grown films was never verified by using any surface composition analysis techniques. Therefore, in order to support this argument, a better understanding of the possible diffusion or evaporation processes of Ir adatoms as well as a better control of the Ir concentration in the films is needed. More experiments in that regard are required to provide evidence for a possible use of Ir to increase surface adatom mobility.

The comparison of the RHEED-intensity relaxation time for a single pulse of Ir-doped $SrTiO_3$ and non-doped $SrTiO_3$ on a $SrTiO_3$ substrate was attempted to examine the immediate effect of Ir species on the surface relaxation. The results show that the relaxation time for the non-doped $SrTiO_3$ pulse is about a third shorter than for Ir:$SrTiO_3$. In addition, using a Ir:$SrTiO_3$ film on top of a $SrTiO_3$ substrate showed an even longer relaxation time. However, analyzing the first pulse of other deposition data revealed that the relaxation times between samples can differ by more than ten times in value. When comparing the RHEED patterns for both the non-doped $SrTiO_3$ one-pulse experiment and the Ir:$SrTiO_3$ one, a difference in the surface morphology was observed. It was therefore concluded that the surface morphology of the substrate is dominating

any possible effect of Ir species on $SrTiO_3$ thin film growth. Thus a detailed knowledge of the underlying substrate surface morphology is crucial before conducting any pulse comparisons.

Since this thesis took inspiration from previous research which investigated the formation of self-assembled Ir nanopillars, the Ir segregation mechanisms for the deposition parameters used in the growth mode experiments from the literature were investigated. Nano-scale clusters with similar features as those reported in the literature were reproduced for one experiment using multiple intermediate deposition steps. In AFM discernible clusters for 600 °C were only observed when using a repetition rate of 1 Hz and depositing 720 pulses. Using a lower repetition rate of 0.25 Hz while depositing the same amount of pulses, showed no visible clustering on the surface. Diffusion of the Ir species into the bulk which prohibits the clusters from reaching the stabilizing critical cluster size due to a longer diffusion time between two pulses, remains the best explanation for their absence. In order to determine the actual Ir concentration of the films and whether the clusters are indeed nanopillars, surface composition analysis techniques are required. These experiments could explain the origin of the non-visible clustering on the surface.

This thesis demonstrated the challenges of conducting PLD thin film growth experiments which compare the effects of using doped versus undoped targets and highlighted the importance of growth parameters such as the laser repetition rate, the substrate-surface morphology and the dopant concentration in the films. However, the results also point at a difference in the surface migration rate between Ir:$SrTiO_3$ and non-doped $SrTiO_3$ which could support the initial assumption that Ir can act as a surfactant for $SrTiO_3$ homoepitaxial growth. Further experiments which bring more understanding of the effect of the Ir concentration in the films on the growth mode and the diffusion processes of Ir species could serve as a basis for using Ir as a surfactant for $SrTiO_3$ thin film growth.

Appendices

A Pt:$SrTiO_3$ RHEED intensity curves

A RHEED intensity comparison was attempted for Pt:$SrTiO_3$ with pure $SrTiO_3$ for temperatures 600 °C, 700 °C and 800 °C. The RHEED curves for $SrTiO_3$ show that the set-up was not ideal since there are no well-defined oscillations visible as in the experiments shown in Section 3.3. 800 °C, the RHEED intensity saturated, making it impossible to make qualitative statements about the film growth. The data shows a large discrepancy between the number of pulses needed to complete an entire oscillation for Pt:$SrTiO_3$ and non-doped $SrTiO_3$.

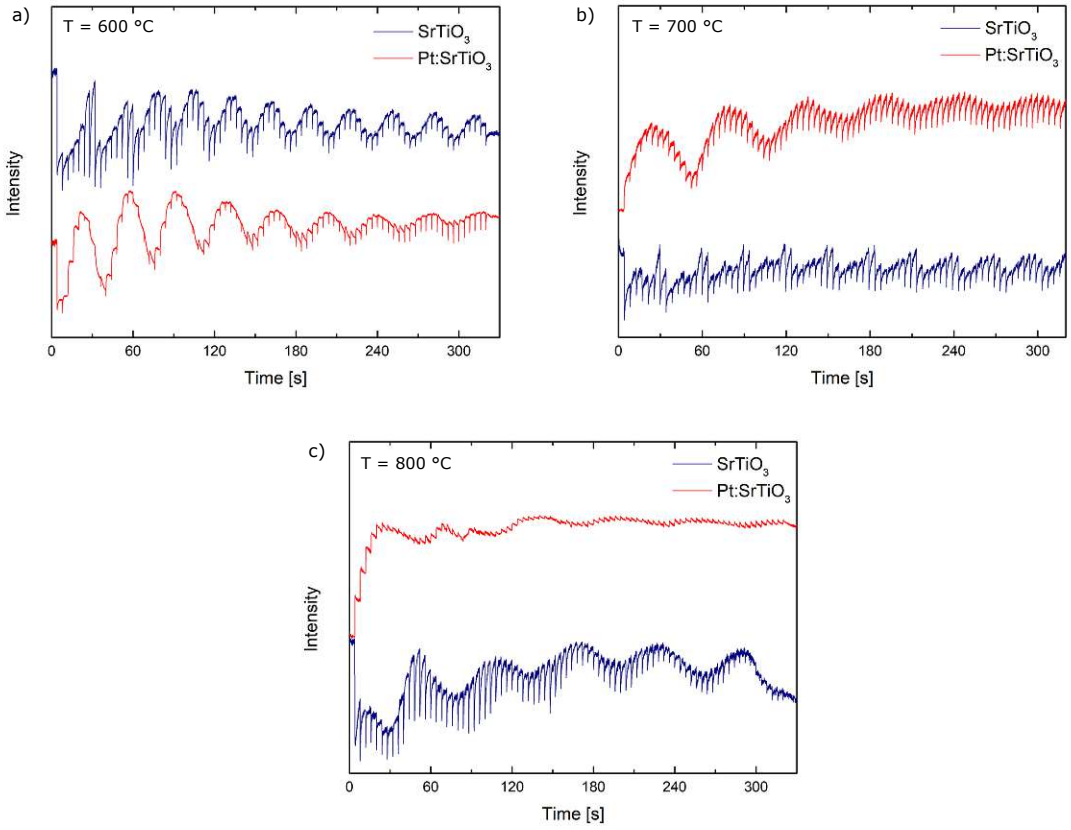

Figure 26: RHEED intensity curve comparisons for Pt:$SrTiO_3$ with undoped $SrTiO_3$ as used target for temperatures a) 600 °C, b) 700 °C and c) 800 °C.

B Relaxation times for $SrTiO_3$ RHEED intensity oscillations

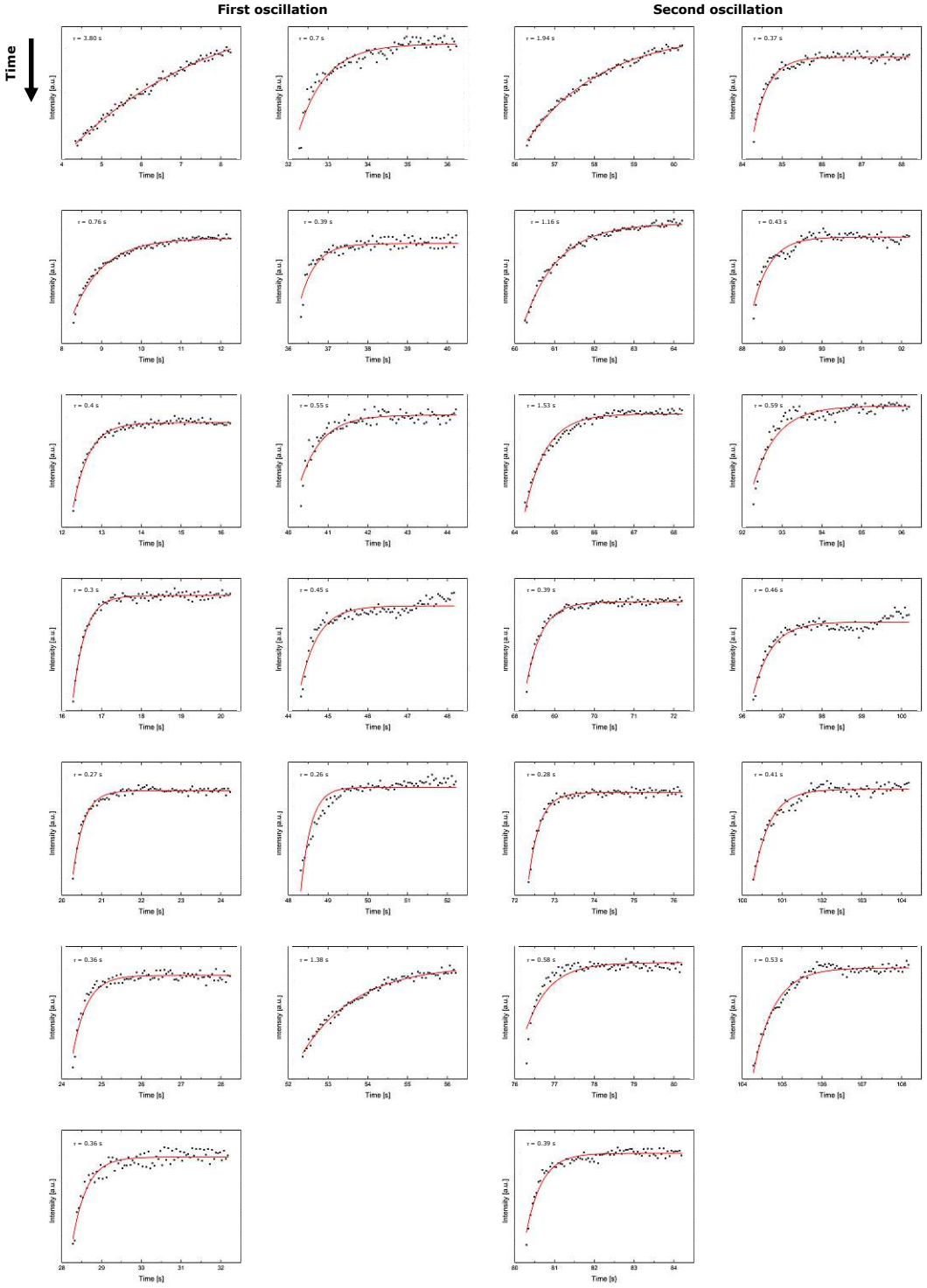

Figure 27: Relaxation times for the first two RHEED intensity oscillations for depositing non-doped $SrTiO_3$ at 800 °C with a repetition rate of 0.25 Hz.

References

[1] U. Diebold, S. C. Li, and M. Schmid, "Oxide surface science," *Annual Review of Physical Chemistry*, vol. 61, p. 129, 2010. doi: 10.1146/annurev.physchem.012809.103254.

[2] M. M. Khan, S. F. Adil, and A. Al-Mayouf, "Metal oxides as photocatalysts," *Journal of Saudi Chemical Society*, vol. 19, p. 462, 2015. doi: 10.1016/j.jscs.2015.04.003.

[3] J. Jupille and G. Thornton, *Defects at Oxide Surfaces*, vol. 58. Springer, 2015.

[4] L. Liu, Y. Jiang, H. Zhao, J. Chen, J. Cheng, K. Yang, and Y. Li, "Engineering co-exposed (001) and (101) facets in oxygen-deficient TiO_2 nanocrystals for enhanced CO_2 photoreduction under visible light," *ACS Catalysis*, vol. 6, no. 2, p. 1097, 2016. doi: 10.1021/acscatal.5b02098.

[5] M. Lippmaa, S. Kawasaki, R. Takahashi, and T. Yamamoto, "Noble metal clustering and nanopillar formation in an oxide matrix," *Japanese Journal of Applied Physics*, vol. 59, no. 1, p. 010501, 2020. doi: 10.7567/1347-4065/ab57e2.

[6] R. Meyer, R. Waser, J. Helmbold, and G. Borchardt, "Cationic surface segregation in donor-doped $SrTiO_3$ under oxidizing conditions," *Journal of Electroceramics*, vol. 9, p. 101, 2002. doi: 10.1023/A:1022898104375.

[7] N. Osawa, R. Takahashi, and M. Lippmaa, "Hole trap state analysis in $SrTiO_3$," *Applied Physics Letters*, vol. 110, no. 26, p. 263902, 2017. doi: 10.1063/1.4991015.

[8] P. Zahl, P. Kury, and M. H. V. Hoegen, "Interplay of surface morphology, strain relief, and surface stress during surfactant mediated epitaxy of Ge on Si," *Applied Physics A*, vol. 69, p. 481, 1999. doi: 10.1007/s003399900170.

[9] A. Picone, A. Brambilla, A. Calloni, L. Duò, M. Finazzi, and F. Ciccacci, "Oxygen-induced effects on the morphology of the Fe(001) surface in out-of-equilibrium conditions," *Physical Review B*, vol. 83, p. 235402, 2011. doi: 10.1103/PhysRevB.83.235402.

[10] M. Setvín, M. Wagner, M. Schmid, G. S. Parkinson, and U. Diebold, "Surface point defects on bulk oxides: Atomically-resolved scanning probe microscopy," *Chemical Society Reviews*, vol. 46, p. 1772, 2017. doi: 10.1039/c7cs00076f.

[11] S. Gerhold, Z. Wang, M. Schmid, and U. Diebold, "Stoichiometry-driven switching between surface reconstructions on $SrTiO_3(001)$," *Surface Science*, vol. 621, p. L1, 2014. doi: 10.1016/j.susc.2013.10.015.

[12] E. J. Tarsa, E. A. Hachfeld, F. T. Quinlan, J. S. Speck, and M. Eddy, "Growth-related stress and surface morphology in homoepitaxial $SrTiO_3$ films," *Applied Physics Letters*, vol. 68, p. 490, 1995. doi: 10.1063/1.116376.

[13] M. Lippmaa, S. Kawasaki, R. Takahashi, and T. Yamamoto, "Nanopillar composite electrodes for solar-driven water splitting," *MRS Bulletin*, vol. 46, p. 142, 2021. doi: 10.1557/s43577-021-00030-6.

[14] M. Lippmaa, N. Nakagawa, M. Kawasaki, S. Ohashi, and H. Koinuma, "Growth mode mapping of $SrTiO_3$ epitaxy," *Applied Physics Letters*, vol. 76, p. 2439, 2000. doi: 10.1063/1.126369.

[15] D. Blank, G. Koster, G. Rijnders, E. van Setten, P. Slycke, and H. Rogalla, "Imposed layer-by-layer growth by pulsed laser interval deposition," *Applied Physics A Materials Science & Processing*, vol. 69, p. 17, 1999. doi: 10.1007/s003399900187.

[16] G. Rijnders and D. H. A. Blank, *Growth Kinetics During Pulsed Laser Deposition*, ch. 8, pp. 177–190. John Wiley & Sons, Ltd, 2006. doi: 10.1002/9780470052129.ch8.

[17] M. C. Sullivan, M. J. Ward, A. Gutiérrez-Llorente, E. R. Adler, H. Joress, A. Woll, and J. D. Brock, "Complex oxide growth using simultaneous in situ reflection high-energy electron diffraction and x-ray reflectivity: When is one layer complete?," *Applied Physics Letters*, vol. 106, p. 031604, 2015. doi: 10.1063/1.4906419.

[18] H. Brune, "Microscopic view of epitaxial metal growth: nucleation and aggregation," *Surface Science Reports*, vol. 31, no. 4-6, p. 121, 1998. doi: 10.1016/S0167-5729(99)80001-6.

[19] K. Oura, *Surface Science An Introduction*. Springer Berling, Heidelberg, 2003.

[20] X. D. Zhu, W. Si, X. X. Xi, and Q. Jiang, "Oxidation kinetics in $SrTiO_3$ homoepitaxy," *Materials Research Society Symposium - Proceedings*, vol. 619, p. 115, 2000. doi: 10.1063/1.1338497.

[21] G. Rijnders and D. H. A. Blank, *Growth Kinetics During Pulsed Laser Deposition*, ch. 8, p. 177. John Wiley & Sons, Ltd, 2006. doi: https://doi.org/10.1002/9780470052129.ch8.

[22] C. Ratsch and J. A. Venables, "Nucleation theory and the early stages of thin film growth," *Journal of Vacuum Science & Technology A*, vol. 21, no. 5, p. 96, 2003. doi: 10.1116/1.1600454.

[23] J. W. Evans, M. Li, and M. C. Bartelt, "Rate equation theory for island sizes and capture zone areas in submonolayer deposition: Realistic treatment of spatial aspects of nucleation," *MRS Online Proceedings Library*, vol. 749, p. 22, 2003. doi: 10.1557/PROC-749-W2.2.

[24] V. Gabriel, P. Kocán, and V. Holý, "Effective algorithm for simulations of layer-by-layer growth during pulsed-laser deposition," *Physical Review E*, vol. 102, p. 063305, 2020. doi: 10.1103/PhysRevE.102.063305.

[25] C. Ratsch, M. F. Gyure, R. E. Caflisch, F. Gibou, M. Petersen, M. Kang, J. Garcia, and D. D. Vvedensky, "Level-set method for island dynamics in epitaxial growth," *Physical Review B*, vol. 65, p. 195403, 2002. doi: 10.1103/PhysRevB.65.195403.

[26] V. Gabriel, P. Kocán, and V. Holý, "Growth-rate model of epitaxial layer-by-layer growth by pulsed-laser deposition," *Physical Review E*, vol. 106, p. 035302, 2022. doi: 10.1103/PhysRevE.106.035302.

[27] Z. Zhang and M. G. Lagally, "Atomistic processes in the early stages of thin-film growth," *Science*, vol. 276, no. 5311, p. 377, 1997. doi: 10.1126/science.276.5311.377.

[28] R. Q. Hwang, C. Günther, J. Schröder, S. Günther, E. Kopatzki, and R. J. Behm, "Nucleation and growth of thin metal films on clean and modified metal substrates studied by scanning tunneling microscopy," *Journal of Vacuum Science & Technology A*, vol. 10, no. 4, p. 1970, 1992. doi: 10.1116/1.578012.

[29] A. Rijnders, *The initial growth of complex oxides: study and manipulation*. PhD thesis, University of Twente, Netherlands, 2001.

[30] G. Koster, *Artificially layered oxides by pulsed laser deposition*. PhD thesis, University of Twente, Netherlands, 1999.

[31] J. H. Haeni, P. Irvin, W. Chang, R. Uecker, P. Reiche, Y. L. Li, S. Choudhury, W. Tian, M. E. Hawley, B. Craigo, A. K. Tagantsev, X. Q. Pan, S. K. Streiffer, L. Q. Chen, S. W. Kirchoefer, J. Levy, and D. G. Schlom, "Room-temperature ferroelectricity in strained $SrTiO_3$," *Nature*, vol. 430, p. 758, 2004. doi: 10.1038/nature02773.

[32] Z. Zhang, P. Qian, X. Yang, B. Wu, H. L. Cai, F. M. Zhang, and X. S. Wu, "Manipulating the carrier concentration and phase transition via Nb content in $SrTiO_3$," *Scientific Reports*, vol. 12, p. 2045, 2022. doi: 10.1038/s41598-021-03199-7.

[33] S. Kawasaki, K. Nakatsuji, J. Yoshinobu, F. Komori, R. Takahashi, M. Lippmaa, K. Mase, and A. Kudo, "Epitaxial Rh-doped $SrTiO_3$ thin film photocathode for water splitting under visible light irradiation," *Applied Physics Letters*, vol. 101, p. 033910, 2012. doi: 10.1063/1.4738371.

[34] C. Wang, H. Qiu, T. Inoue, and Q. Yao, "Band gap engineering of srtio3 for water splitting under visible light irradiation," *International Journal of Hydrogen Energy*, vol. 39, p. 12507, 2014. doi: 10.1016/j.ijhydene.2014.06.059.

[35] R. Konta, T. Ishii, H. Kato, and A. Kudo, "Photocatalytic activities of noble metal ion doped $SrTiO_3$ under visible light irradiation," *Journal of Physical Chemistry B*, vol. 108, p. 8992, 2004. doi: 10.1021/jp049556p.

[36] D. H. Murthy, H. Matsuzaki, Q. Wang, Y. Suzuki, K. Seki, T. Hisatomi, T. Yamada, A. Kudo, K. Domen, and A. Furube, "Revealing the role of the Rh valence state, La doping level and Ru cocatalyst in determining the H_2 evolution efficiency in doped $SrTiO_3$ photocatalysts," *Sustainable Energy and Fuels*, vol. 3, p. 208, 2019. doi: 10.1039/c8se00487k.

[37] C. Cheng and R. Long, "Charge-compensated doping extends carrier lifetimes in $SrTiO_3$ by passivating oxygen vacancy defects," *Journal of Physical Chemistry Letters*, vol. 12, p. 12040, 2021. doi: 10.1021/acs.jpclett.1c03775.

[38] M. Kawasaki, K. Takahashi, T. Maeda, R. Tsuchiya, M. Shinohara, O. Ishiyama, T. Yonezawa, M. Yoshimoto, and H. Koinuma, "Atomic control of the $SrTiO_3$ crystal surface," *Proceedings of the National Academy of Sciences of the United States of America*, vol. 31, p. 235, 1994. doi: 10.1126/science.266.5190.1540.

[39] G. Koster, B. L. Kropman, G. J. Rijnders, D. H. Blank, and H. Rogalla, "Quasi-ideal strontium titanate crystal surfaces through formation of strontium hydroxide," *Applied Physics Letters*, vol. 73, p. 2920, 1998. doi: 10.1063/1.122630.

[40] S. Chambers, T. Droubay, C. Capan, and G. Sun, "Unintentional f doping of srtio3(001) etched in hf acid-structure and electronic properties," *Surface Science*, vol. 606, no. 3, p. 554, 2012. doi: 10.1016/j.susc.2011.11.029.

[41] J. Fompeyrine, R. Berger, H. P. Lang, J. Perret, E. Mächler, C. Gerber, and J. P. Locquet, "Local determination of the stacking sequence of layered materials," *Applied Physics Letters*, vol. 72, p. 1697, 1998. doi: 10.1063/1.121155.

[42] H. Yan, J. M. Börgers, M. A. Rose, C. Baeumer, B. Kim, L. Jin, R. Dittmann, and F. Gunkel, "Stoichiometry and termination control of $LaAlO_3/SrTiO_3$ bilayer interfaces," *Advanced Materials Interfaces*, vol. 8, no. 3, p. 2001477, 2021. doi: 10.1002/admi.202001477.

[43] G. Charlton, S. Brennan, C. Muryn, R. McGrath, D. Norman, T. Turner, and G. Thornton, "Surface relaxation of $SrTiO_3$ (001)," *Surface Science*, vol. 457, no. 1, p. 376, 2000. doi: https://doi.org/10.1016/S0039-6028(00)00403-9.

[44] T. Nishimura, A. Ikeda, H. Namba, T. Morishita, and Y. Kido, "Structure change of tio_2-terminated $SrTiO_3$ (001) surfaces by annealing in O_2 atmosphere and ultrahigh vacuum," *Surface Science*, vol. 421, p. 273, 1999. doi: 10.1016/S0039-6028(98)00840-1.

[45] I. Sokolović, G. Franceschi, Z. Wang, J. Xu, J. Pavelec, M. Riva, M. Schmid, U. Diebold, and M. Setvin, "Quest for a pristine unreconstructed $SrTiO_3$ (001) surface: An atomically resolved study via noncontact atomic force microscopy," *Physical Review B*, vol. 103, p. L241406, 2021. doi: 10.1103/PhysRevB.103.L241406.

[46] W. Braun, *Applied RHEED: Reflection High-Energy Electron Diffraction During Crystal Growth*. Springer Berlin Heidelberg, 1999. doi: 10.1007/BFb0109550.

[47] S. Hasegawa, *Reflection High-Energy Electron Diffraction*, p. 1. John Wiley & Sons, Ltd, 2012. doi: 10.1002/0471266965.com139.

[48] W. Braun, L. Däweritz, and K. H. Ploog, "Origin of electron diffraction oscillations during crystal growth," *Physical Review Letters*, vol. 80, p. 4935, 1998. doi: 10.1103/PhysRevLett.80.4935.

[49] Z. Mitura, S. L. Dudarev, and M. J. Whelan, "Phase of RHEED oscillations," *Physical Review B*, vol. 57, p. 6309, 1998. doi: 10.1103/PhysRevB.57.6309.

[50] D. M. Holmes, J. L. Sudijono, C. F. Mcconville, T. S. Jones, and B. A. Joyce, "Direct evidence for the step density model in the initial stages of the layer-by-layer homoepitaxial growth of GaAs(111)A," *Surface Science*, vol. 370, p. 173, 1997. doi: 10.1016/S0039-6028(96)01173-9.

[51] S. Stoyanov and M. Michailov, "Non-steady state effects in MBE: Oscillations of the step density at the crystal surface," *Surface Science*, vol. 202, no. 1, p. 109, 1988. doi: https://doi.org/10.1016/0039-6028(88)90064-7.

[52] U. Korte and P. A. Maksym, "Role of the step density in reflection high-energy electron diffraction: Questioning the step density model," *Physical Review Letters*, vol. 78, p. 2381, 1997. doi: 10.1103/PhysRevLett.78.2381.

[53] G. Binnig, C. F. Q. ', E. L. Gi, and C. Gerber, "Atomic force microscope," *Physical Review Letters*, vol. 56, p. 930, 1986. doi: 10.1103/physrevlett.56.930.

[54] Q. D. Jiang and J. Zegenhagen, "c(6×2) and c(4×2) reconstruction of $SrTiO_3$ (001)," *Surface Science*, vol. 425, p. 343, 1999. doi: 10.1016/j.susc.2006.05.043.

[55] J. Lee, J. Juang, K. Wu, T. Uen, and Y. Gou, "Temperature dependence of RHEED oscillation in homoepitaxial growth of $SrTiO_3$(100) films on stepped substrates," *Surface Science*, vol. 449, no. 1, p. 235, 2000. doi: 10.1016/S0039-6028(00)00039-X.

[56] M. Riva, G. Franceschi, M. Schmid, and U. Diebold, "Epitaxial growth of complex oxide films: Role of surface reconstructions," *Physical Review Research*, vol. 1, p. 033059, 2019. doi: 10.1103/PhysRevResearch.1.033059.

[57] S. Wicklein, A. Sambri, S. Amoruso, X. Wang, R. Bruzzese, A. Koehl, and R. Dittmann, "Pulsed laser ablation of complex oxides: The role of congruent ablation and preferential scattering for the film stoichiometry," *Applied Physics Letters*, vol. 101, p. 131601, 2012. doi: https://doi.org/10.1063/1.4754112.

[58] T. Ohnishi, K. Shibuya, T. Yamamoto, and M. Lippmaa, "Defects and transport in complex oxide thin films," *Journal of Applied Physics*, vol. 103, p. 103703, 2008. doi: 10.1063/1.2921972.

[59] G. Franceschi, M. Wagner, J. Hofinger, T. c. v. Krajňák, M. Schmid, U. Diebold, and M. Riva, "Growth of In_2O_3(111) thin films with optimized surfaces," *Physical Review Materials*, vol. 3, p. 103403, 2019. doi: 10.1103/PhysRevMaterials.3.103403.

[60] F. Kraushofer and G. S. Parkinson, "Single-atom catalysis: Insights from model systems," *Chemical Reviews*, vol. 122, no. 18, p. 14911, 2022. doi: 10.1021/acs.chemrev.2c00259.

[61] S. Kawasaki, R. Takahashi, T. Yamamoto, M. Kobayashi, H. Kumigashira, J. Yoshinobu, F. Komori, A. Kudo, and M. Lippmaa, "Photoelectrochemical water splitting enhanced by self-assembled metal nanopillars embedded in an oxide semiconductor photoelectrode," *Nature Communications*, vol. 7, p. 11818, 2016. doi: 10.1038/ncomms11818.

[62] M. Lee, R. Arras, R. Takahashi, B. Warot-Fonrose, H. Daimon, M.-J. Casanove, and M. Lippmaa, "Noble metal nanocluster formation in epitaxial perovskite thin films," *ACS Omega*, vol. 3, no. 2, p. 2169, 2018. doi: 10.1021/acsomega.7b02071.